GROUND EFFECT MODELS FOR ROTORCRAFT/SHIP DYNAMIC INTERFACE STUDY

J.V.R. Prasad
L.N. Sankar
School of Aerospace Engineering
Georgia Institute of Technology
Atlanta, GA 30332

Project Final Report
Contract #: N62269-90-C-0246

Submitted to:
Naval Air Warfare Center
Warminister, PA 18974-0591

April 1996

SUMMARY

A real time simulation model of ship ground effect for rotorcraft/ship dynamic interactions is developed by combining computational fluid dynamics (CFD) analysis and finite state representation of rotor inflow. For CFD analysis, the ship is modeled using a source panel representation and the rotor wake is modeled as rigid with prescribed geometry but unknown vorticity distribution. The sea surface is modeled by placing an image rotor wake and an image ship panel system below the sea surface. The CFD model is then combined with a batch version of a generic flight simulation program. From trim solutions using the simulation program, the ship ground effect on rotor inflow for cases of helicopter hovering with respect to ship deck at different points are identified and analyzed. With finite state representation of rotor inflow, a real time simulation model of ship ground effect is developed using in-ground effect inflow results from the CFD analysis.

INTRODUCTION

Modern helicopters must routinely operate from various naval ships under adverse weather conditions, including high winds, high seas, and low visibility. Under many combinations of such conditions, and for various ship orientations relative to the wind and waves, helicopter launch and recovery operations prove unsafe. Safe operating envelopes thus must be determined for each particular helicopter and ship combination. Current methodology to determine such envelopes involves extensive flight testing at sea. However, with an ever increasing number of rotorcraft and ship combinations, it has become prohibitive, both economically and operationally, to carry out testing at sea on the entire test matrix of U.S. Navy, Marine Corps, and Coast Guard rotorcraft aboard U.S. Navy and Coast Guard ships. It has been recognized for some time that an attractive alternative to full scale testing would be to perform the bulk of rotorcraft launch and recovery envelope expansion using real time piloted simulation.

An important ingredient of simulation models that can be used for rotorcraft/ship dynamic interface study is adequate representation of ground effect between the ship deck and the vehicle for simulation of shipboard landing and take off maneuvers. Current simulation models include empirically derived ground effect models which are basically quasi-steady in nature, i.e., the uniform part of the rotor downwash and the rotor thrust are modeled as functions of instantaneous vertical height from the ship deck. The ground effect model suitable for simulation of shipboard operations must include effects that result from rolling, pitching and heaving motions of the ship deck. Also, the ground effect model needs be computationally simple to be included in a real time rotorcraft flight simulation for man-in-the-loop simulation studies in order to determine handling qualities and pilot workload during shipboard operations. This report documents results from the research effort carried out in the School of Aerospace Engineering at the Georgia Institute of Technology on the development of a real time simulation model of ship ground effect.

MODEL DEVELOPMENT AND RESULTS

The general methodology used for developing a real time simulation model of ship ground effect is as follows. First, a comprehensive computational fluid dynamic (CFD) model that takes into account interactions between rotor wake and ship deck, super structure and sea surface is developed. The CFD model is then combined with a comprehensive non-real time helicopter simulation model. Rotor inflow distributions for cases of helicopter trimmed at different points with respect to ship deck with different values of ship speed are obtained. Then a harmonic analysis of inflow distribution for each of the cases is carried out. Using results from the harmonic analysis, the gain matrix of the

dynamic inflow model is modified by matching the inflow distribution predicted by the dynamic inflow model with CFD results.

The general methodology was applied for the development of a real time ship ground effect simulation model of the SH-60 helicopter hovering over the deck of a FFG-7 class frigate. The models developed and the results obtained have been presented at various conferences and the same are included as Appendices.

Appendix 1: Mello, O.A.F., Prasad, J.V.R., Sankar, L.N. and Tseng, W., 'Analysis of Helicopter/Ship Aerodynamic Interactions," Paper presented at the 1994 AHS Aeromechanics Specialists Conference, San Francisco, January 1994.

This paper documents the CFD model development using a prescribed wake approach. Both the geometry and the vortex distribution in the rotor wake are prescribed. Results of inflow distributions and control positions required for trim are included.

Appendix 2: Zhang, H., Mello, O.A.F., Prasad, J.V.R., Sankar, L.N. and Funk, J.D., "A Simulation Model of Ship Ground Effect for Rotorcraft/Ship Interaction Study," Paper presented at the 1995 AHS Forum.

This paper modifies the CFD model by treating the vortex distribution as unknown and determined as part of the solution. Also, it documents the development of a real time ship ground effect simulation model using a finite state wake representation for the SH-60 helicopter hovering over the ship deck moving at a speed of 15 knots.

Appendix 3: Zhang, H., Prasad, J.V.R., Sankar, L.N., Mello, O.A.F. and Funk, J.D., "Ground Effect Simulation Model for Rotorcraft/Ship Interaction Study," Paper presented at the AIAA Flight Simulation Conference, August 1995.

This paper describes the general methodology used for the development of a real time ship ground effect simulation model and includes results for various values of ship speed. Also, it includes results on effects of wake parameters used in the CFD model (wake clearance and number of rotor revolutions of wake) on rotor power.

Appendix 4:

This appendix details the batch version of the ship ground effect simulation model computer code with details on mathematical model development.

CONCLUSIONS

The following conclusions can be made from the results of this study:

1. It is possible to develop a dynamic inflow model, which is applicable to in-ground effect flight conditions, by appropriately adjusting the parameters (of M and L matrices) of the dynamic inflow model.

2. The developed model is found to take into account of 'partial ground effect' as seen in the case of a rotor hovering over the edge of a ship deck.

FUTURE WORK

1. The present study addresses only steady state (trimmed flight) cases. Further work is needed for the unsteady case of heaving, pitching and rolling ship deck.

2. Validation of the model using experimental data is needed.

APPENDIX 1

ANALYSIS OF HELICOPTER / SHIP AERODYNAMIC INTERACTIONS

O. A. F. Mello[*],   J. V. R. Prasad,   L. N. Sankar   and   W. Tseng
Graduate Student   Associate Professor   Professor   Aerospace Engineer
                 School of Aerospace Engineering   Naval Air Warfare Center
                 Georgia Institute of Technology   Aircraft Division
                      Atlanta, Georgia   Warminster, Pennsylvania

ABSTRACT

A method for analysis of the aerodynamic interactions between a helicopter and a ship is presented. The complex flow problem is decomposed into two: The first effect is the ship "ground effect", consisting of the changes in the helicopter-induced flowfield in the vicinity of the ship so that the airflow contours the ship surface. This effect is modeled by a panel representation of the ship surface, taking into account the downwash induced by the rotor and its wake. The second effect is the ship airwake effect, for which a recently developed model at Georgia Institute of Technology, derived from full-scale measurements, is used. This airwake model provides both mean and turbulent velocity components. Numerical results for a SH-60 helicopter trimmed at several locations near a FFG-7 class frigate are presented and these results indicate that both effects are quantitatively important and need to be considered in realistic simulations.

INTRODUCTION

Landing a helicopter on a ship deck can be a hazardous process. The determination of safe operating envelopes has been done at sea in a lengthy and expensive process[1]. The need to consider the many combinations of ships and helicopters aggravates the problem and suggests a demand for an appropriate helicopter/ship aerodynamic interaction model to be incorporated into rotorcraft simulation codes.

There are several aspects that contribute to the complexity of the problem, namely:
1. Sea and ship motions;
2. Atmospheric turbulence;
3. Ship aerodynamics;
4. Helicopter motion itself, in the presence of the ship.

The sea and ship motions can be modeled to a reasonable degree[2]. The only effect of the sea motion on the helicopter would be in the extent that it modifies the ground effect, but this change may be regarded as negligible with respect to the other factors involved. The ship motion will have a more significant effect on the ship/helicopter interference and has to be considered.

The ship aerodynamics is very complex. The flow around the superstructure is characterized by turbulence and vortex shedding. The turbulence level in the atmosphere also affects the flow. The knowledge about this type of flow is mostly empirical and based on building aerodynamics. During the past few years, there has been an increased activity in investigating the ship airwake through wind-tunnel[3-5] and full-scale[6-7] tests. A recent research effort by Prasad et al.[8] has used full-scale ship airwake measurements obtained by the Australian Aeronautical Research Laboratory[7] to construct a quantitative model of the ship airwake using system identification techniques.

In the present approach, the effects of ship aerodynamics on the helicopter are divided into the "ground effect" due to the proximity between the rotor and the ship surface, and the ship airwake effect. The ship "ground effect" is approximately modeled under the assumption of attached flow around the ship, which is subject to the velocity field induced by the rotor and its wake. For this purpose, a panel method representation of the ship surface is used, and the effect of the ship on the rotor is modeled by the induced velocity field produced by the ship's panels.

The ship airwake effect is included using the model developed by Prasad et al.[8], which gives both the mean and turbulent velocity components.

The simulation of helicopter motion near the ship can be carried out by a standard helicopter simulation code, if the effects discussed above are included. The simulation program used in the present work is a general helicopter flight simulation code[9], which uses a blade-element rotor model, suitable for the addition of induced velocity components due to the ship panel system and velocity components from the ship airwake model.

The remaining of this paper is organized as follows: First, a brief description of the mathematical formulation of the rotor wake and ship panel methods is given. Next, numerical results for a SH-60 helicopter trimmed at several

locations near a FFG-7 class frigate are presented. The paper concludes with an assessment of the ship "ground" and airwake effects and directions for future work.

MATHEMATICAL FORMULATION

Rotor Wake Formulation

In order to compute the downwash on the ship surface due to the rotor, a rigid wake model is used. The rotor blade is modeled by a lifting line of bound vorticity, which is assumed to have a prescribed variation both radially and azimuth-wise. The wake has a prescribed geometry, which is basically a classical skewed helical wake, with a limited wake contraction model. The wake is divided into a "near" wake, composed of trailing and shed vortices and a "far" wake composed of trailing tip vortices only. The strength of the trailing and shed vortices are given by the radial and azimuth-wise variations of the bound vorticity, respectively, while the strength of the far wake tip vortex is assumed as equal to the maximum bound vorticity at the azimuth location where the vortex filament leaves the blade. The rotor wake is convected downstream with a velocity which is equal to the vector sum of the free stream velocity and the averaged (momentum theory value) induced velocity over the disk.

The blade bound vorticity distribution is assumed to be a known function of the non-dimensional radial location $\bar{r} = r/R$ and azimuth ψ. The radial variation is assumed to be of the form:

$$f(\bar{r}) = \bar{r} \sqrt{1 - \bar{r}^2} \qquad (1)$$

which is characteristic of a typical radial variation of circulation. The azimuth-wise variation is assumed to be such that no thrust offset is produced, by imposing the condition that the total blade moment be constant over the disk[10]. Under this assumption, the resulting azimuth-wise variation can be shown to be:

$$g(\psi) = \frac{1}{1 + \frac{3}{2} k_T \mu \sin \psi} \qquad (2)$$

where ψ is the azimuth, μ is the advance ratio and k_T is a constant which depends on the radial circulation distribution. It can be shown that for the radial variation assumed here, k_T has the value of $15\pi/16$ or approximately 0.982.

With the assumptions (1) and (2), the bound vorticity distribution along the blade and disk is of the form:

$$\Gamma_b(\bar{r}, \psi) = \Gamma_0 \, \bar{r} \sqrt{1 - \bar{r}^2} \, \frac{1}{1 + \frac{3}{2} k_T \mu \sin \psi} \qquad (3)$$

The constant Γ_0 which appears in Eq. (3) may be related to the thrust coefficient C_T by applying the Kutta-Joukowski theorem for a section of the rotor blade and integrating over the rotor disk, which yields:

$$\tilde{\Gamma}_0 = \frac{\Gamma_0}{R(\Omega R)} = C_T \frac{\pi}{N_b} \frac{\sqrt{1 - a^2}}{\frac{\pi}{16} + \frac{4}{9k_T}(\sqrt{1 - a^2} - 1)} \qquad (4)$$

where $a = 1.5 \, k_T \, \mu$ and N_b is the number of blades.

From Eq. (4), the trailing and shed vorticities in the near wake can be shown to be given respectively by:

$$\Gamma_t(\bar{r}, \psi) = \frac{\partial \Gamma_b}{\partial \bar{r}} = \Gamma_0 \frac{1 - 2\bar{r}^2}{\sqrt{1 - \bar{r}^2}} \frac{1}{1 + \frac{3}{2} k_T \mu \sin \psi} \qquad (5)$$

and

$$\Gamma_s(\bar{r}, \psi) = \frac{\partial \Gamma_b}{\partial \psi} = - \Gamma_0 \, \bar{r} \sqrt{1 - \bar{r}^2} \, \frac{\frac{3}{2} k_T \mu \cos \psi}{\left(1 + \frac{3}{2} k_T \mu \sin \psi\right)^2} \qquad (6)$$

while the far wake's single trailing tip vortex strength is given by

$$\Gamma_T(\psi) = \frac{1}{2} \Gamma_0 \frac{1}{1 + \frac{3}{2} k_T \mu \sin \psi} \qquad (7)$$

Using the vorticity strengths given by Eqs. (3)–(7) and the assumed wake geometry, the velocities induced by the rotor and its wake on the ship surface are computed by applying the Biot-Savart law and integrating over the radial direction (bound vortices and near wake shed and trailing vortices) and over the wake[11]. The total induced velocities are then resolved for the component normal to the ship panel for input in the ship model.

A crude wake contraction model is applied, such that the near wake initially starts from the blade root cut-out location $\bar{r}_i$ and extends to the blade tip; after the wake shed and trailing vortices have traveled a specified helical angle denoted by v_{ctr}, the wake is contracted such as to start from the hub (r=0) and extend to the radial location r_{tv}. Between $v=0°$ and $v=v_{ctr}$, a linear interpolation is used to determine the starting and end radial locations.

A Rankine vortex core model[12] with radius of one tenth of the blade chord is used. This model is applied by scaling the induced velocity due to the elementary vortex filament by the square of the ratio between the distance to the filament and the core radius, whenever the point where the induced velocity is being calculated lies within the vortex core.

Ship Formulation

The ship is modeled by a source panel method[13] common in aeronautical applications. The ship surface is approximately represented by plane source panels with constant distributed strength. The strengths of the sources are determined by enforcing the non-penetration condition at the centroid of each panel. A typical ship panel representation is shown in Fig. 1.
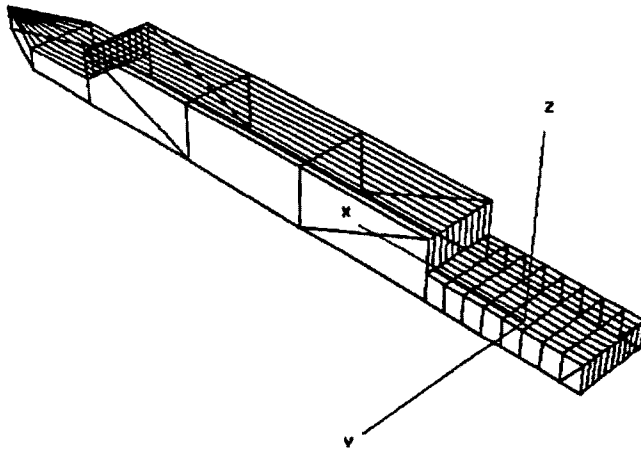
Fig. 1: Ship Panel Representation.

Since the ship airwake mean velocities are given by polynomial fitting of full-scale measurements, the ship's mean velocity is not considered for computation of the right-hand side of the system of equations, i.e., only the component of the downwash induced by the rotor normal to the ship panel and the normal component of the ship's oscillatory motion are taken into account in this implementation. This formulation results in a linear system of equations which is solved for the source strengths σ:

$$[A]\{\sigma\} = [B] \qquad (8)$$

where [A] is the matrix of influence coefficients, {σ} is the vector of unknown source strengths and [B] is the right-hand side which includes the normal component of the velocities on the ship surface due to ship oscillatory motion and due to the rotor and its wake. The system of equations (8) is solved by a standard LU decomposition for efficient backsubstitution at each time step. The resulting source

panel strengths are then used to compute the velocities induced by the ship source panel system on the rotor disk.

Effect of Sea Surface

In order to model the ground effect due to the sea surface, the method of images is used. An image rotor wake and an image ship panel system are placed below the sea surface and the influence of these images is taken into account in the computation of the downwash induced by the rotor and in the computation of the coefficient matrix for the ship panel method.

RESULTS AND DISCUSSION

The above described helicopter/ship interaction method has been applied to a SH-60 Sea Hawk helicopter flying at 15 kts (7.72 m/s) and at a height of one rotor radius (26.83 ft or 8.18 m) above the landing deck of a FFG-7 class frigate. The helicopter was positioned above the center of the deck, above the edge of the deck and at the same height just outside the deck. These positions are illustrated in Fig. 2. The ship was moving forward at the same speed as the helicopter. These positions were chosen as representatives of configurations experienced during the final approach for landing[14]. The helicopter was trimmed at each of the above positions. Note that for trim only the mean component of the ship airwake is used, i.e., the results presented herein do not include the turbulent component.
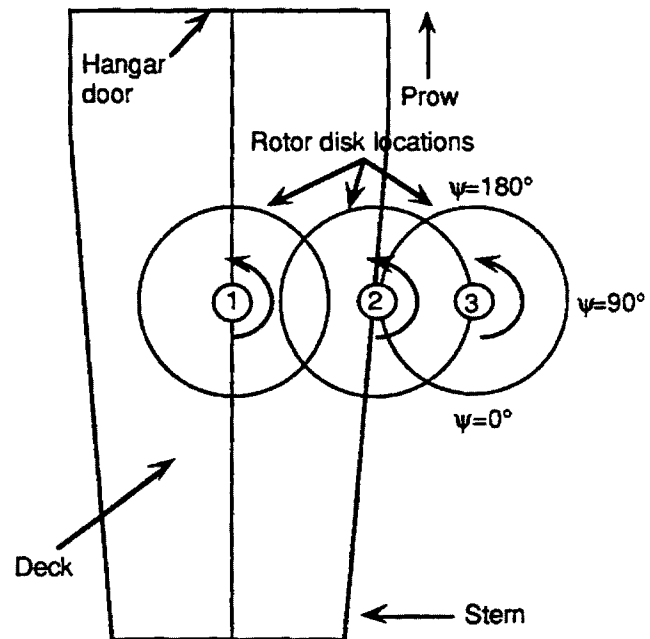

Fig. 2: Positioning of helicopter near ship (top view): Above center of deck (1), above edge of deck (2), and just outside deck (3).
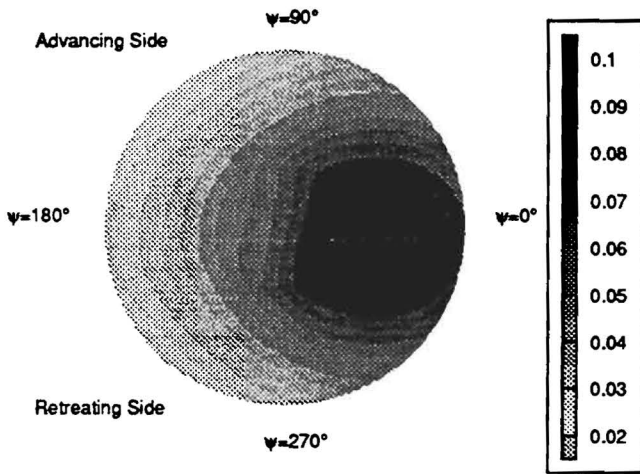
Fig. 3: Normalized upwash induced by ship panel system, helicopter above center of deck.
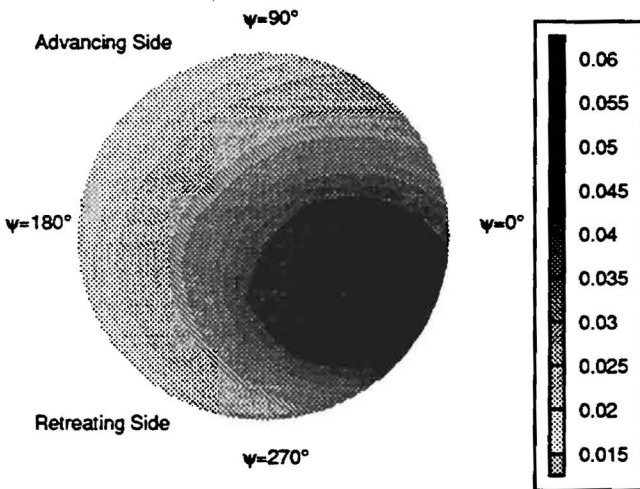

Fig. 4: Normalized upwash induced by ship panel system, helicopter above edge of deck.
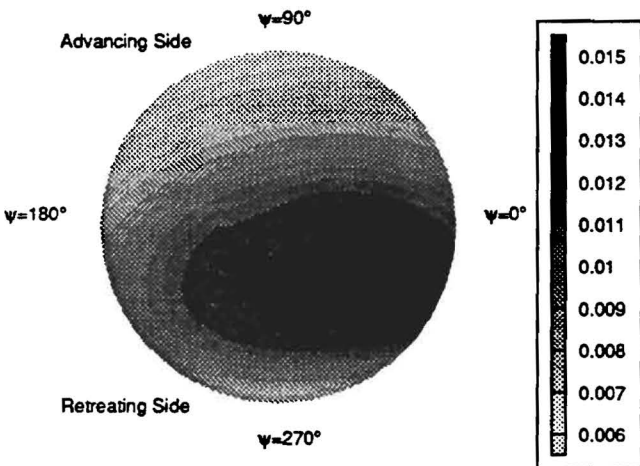

Fig. 5: Normalized upwash induced by ship panel system, helicopter outside deck.

Numerical results for the upwash induced by the ship panel system over the rotor disk, normalized by the mean induced inflow, are presented in Figs. 3–5 for each of the above described helicopter locations. It can be observed that the upwash is generally higher in the aft portion of the disk. This observation can be attributed to the rotor wake being washed aft and consequently the rear portion of the ship deck being more affected by the wake and thus resulting in higher upwash values near that region.

It can also be observed that the upwash is higher in the retreating side of the disk, when the helicopter is moved towards the edge of the deck. This is expected because this part of the rotor disk is closer to the ship deck for this configuration.
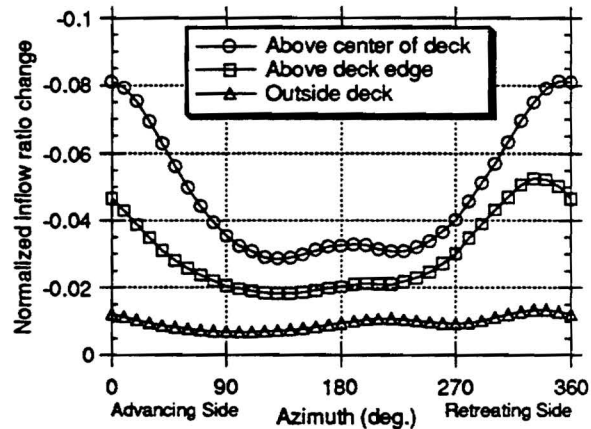

Fig. 6: Effect of helicopter position on ship "ground effect".

The ship "ground effect" can be further visualized in Fig. 6, where the inflow ratio due to the ship panel system, normalized by the mean induced inflow ratio, is presented for each of the above described positions at the radial station 80% and at azimuth locations corresponding to one rotor revolution. For the rotor located just outside the deck, the "ground effect" upwash is mostly uniform and about 1% of the mean induced inflow. As the helicopter moves inward with respect to the deck, the ground effect increases, as expected. It is also clear that the highest values of ship ground effect upwash occur around the aft portion of the disk, as mentioned before.

In current simulation codes[9], it is common to adopt a simple correction factor, based on the height above the ground, to account for the ground effect. While this may be acceptable in other situations, the helicopter-above-ship configuration poses the need for a more accurate local correction. This can be observed in Fig. 7, where the inflow ratio due to the ship panel system, divided by the local inflow ratio, is presented for each of the above described positions at the radial station 80%. It is clear that using a

constant inflow correction factor cannot account for the significant variations involved.
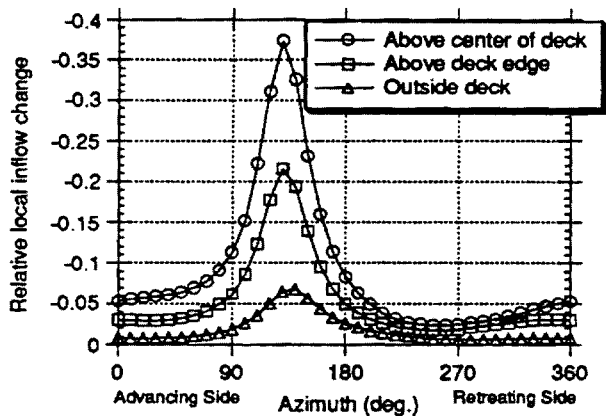

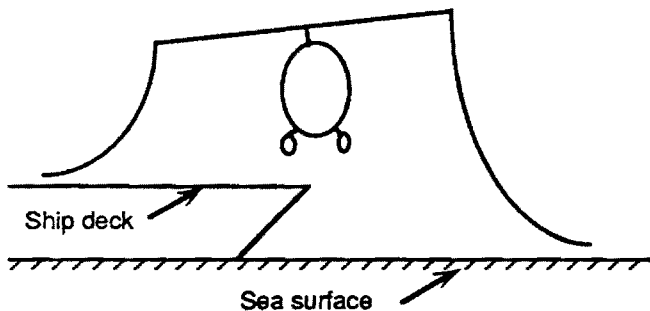Fig. 7: Local inflow change due to ship "ground effect".

Fig. 8: "Partial" Ground Effect

The above discussed results indicate that the distribution of ship ground effect over the disk is very sensitive to the rotor disk location with respect to the deck when the helicopter moves inward for landing, while the magnitude of this effect depends directly on how much of the ship is "washed" by the rotor wake. These phenomena constitute what may be termed as "partial" ground effect, which is shown schematically in Fig. 8. It is clear that this effect should be adequately included in simulations in order to provide increased fidelity. The present method is a tool that can be used to represent this effect. However, during the course of this work it was observed that the computational times required for the current method (about 0.6 CPU sec per iteration in an HP Apollo 700 workstation) are not compatible with a real-time simulation. For example, the time step used in the present calculations was about 0.013 sec. This observation suggests a need for the development of an approximate method that can account for the above described "partial" ground effect. The present method can then be used for parametric studies which will lead to the definition of the important parameters to be included in the approximate real-time simulation method.
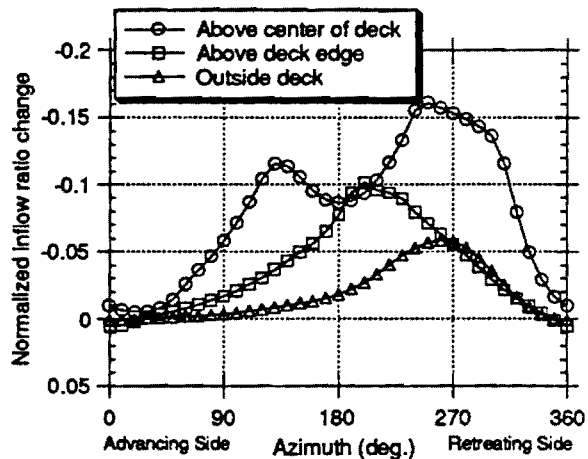

Fig. 9: Effect of helicopter position on normal velocities due to the ship airwake.

In order to compare quantitatively the ship "ground effect" with the ship airwake effect, the contribution of the mean ship airwake to the total inflow ratio, normalized by the mean induced inflow ratio, is presented in Fig. 9 for each of the above described positions at the radial station 80%. It can be observed that the ship airwake contribution is of the same order as the ship ground effect. It should be pointed out that the ship airwake semi-empirical model used here is strictly valid only within the spatial range of coordinates where the velocities were measured during the full-scale tests. Their extrapolation using the same polynomials outside the range is not valid. In order to estimate the effect of the ship airwake outside the valid range and therefore allow a comparison with the ship ground effect, an exponential decay was assumed.
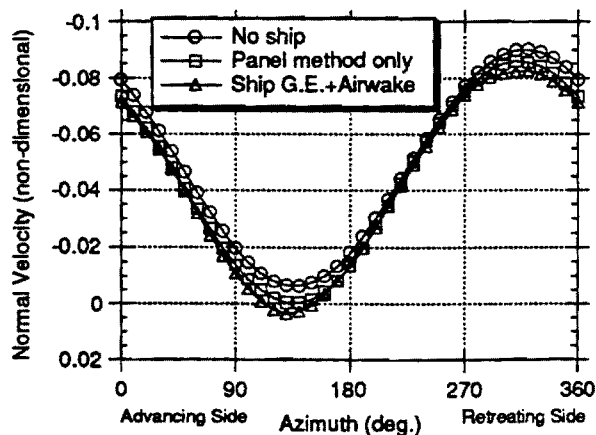

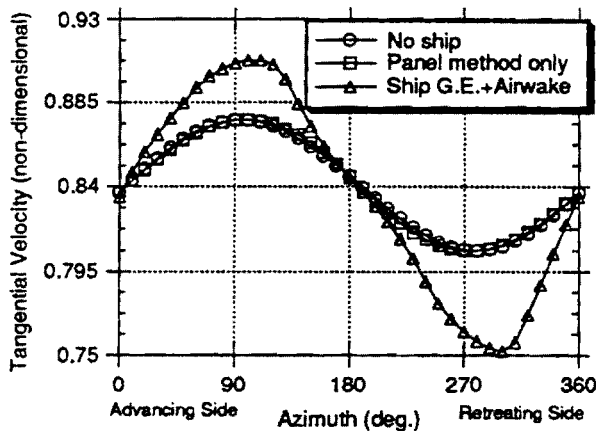Fig. 10: Total normal blade velocities at r/R=0.8, helicopter above center of deck.

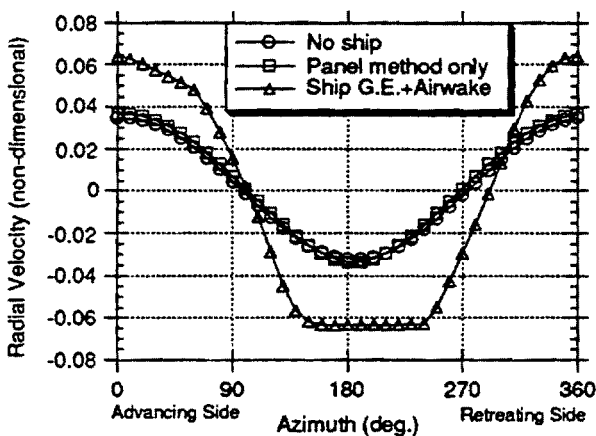Fig. 11: Total tangential blade velocities at r/R=0.8, helicopter above center of deck.

Fig. 12: Total radial blade velocities at r/R=0.8, helicopter above center of deck.

The effects of the ship airwake can be further illustrated by Figs. 10–12, where the total blade normal, tangential and radial velocities, respectively, are presented. The velocities were computed without the ship present, with the ship influence computed using a panel method only, i.e., including the ship free-stream velocity in the computation of the ship sources/sinks, and with the ship airwake in addition to the ship ground effect. While the previously discussed influence of ship ground effect and normal component of airwake is again clear in Fig. 10, the most dramatic effect appears in the tangential and radial components. In general, the ship airwake contributes with an overall increase in forward velocity, although its actual quantitative effect is somewhat localized, which is characteristic of the airwake.

It is clear from Figs. 11–12 that the ship airwake cannot be even crudely approximated by a panel method. Therefore, a ship airwake database is needed in order to provide a realistic simulation.

Table 1: Trimmed Control Positions (inches)

Config	Lat.Cyc.	Long.Cyc.	Collective	Pedal
1	4.595	4.466	5.137	2.008
2	4.595	4.469	5.135	2.010
3	4.563	4.196	4.946	2.084
4	4.622	4.301	5.083	2.072
5	4.599	4.414	5.138	2.037

The overall effect of the modified blade velocities is reflected in the trimmed control positions, as shown in Table 1, where the control positions are shown for five conditions: (1) no ship, no ground effect; (2) no ship, ground effect computed using simple inflow correction[9]; (3) helicopter above center of ship deck; (4) helicopter above edge of ship deck; and (5) helicopter just outside deck. The conventions for these control positions are as follows: full left lateral cyclic corresponds to zero, full right corresponds to 10 in; full forward longitudinal cyclic corresponds to zero, full aft to 10 in; full low collective pitch corresponds to zero, full high to 10 in; full left pedal corresponds to zero, full right to 5.38 in. The increased tangential velocity due to the ship airwake is felt as an addition to the forward velocity, resulting in additional forward longitudinal cyclic as the helicopter moves inward. The lateral cyclic and pedal are also adjusted. The combination of ship ground effect and normal airwake velocity results in decreased collective pitch, which is also more significant when the helicopter moves toward the center of the deck.

CONCLUDING REMARKS

A method for analysis of the aerodynamic interactions between a helicopter and a ship has been presented. This method divides the interaction problem into two effects: the ship "ground effect", modeled by a panel representation of the ship surface, which results in an upwash on the rotor disk, and the ship airwake effect, for which an existing semi-empirical model, derived from full-scale measurements, is used.

Numerical results for a SH-60 helicopter trimmed at three locations near a FFG-7 class frigate have indicated that the ship "ground effect" increases significantly as the helicopter moves toward the center of the ship deck, while its distribution over the disk is sensible to the helicopter location, with higher upwash in the rear portion of the disk

and in the side near the ship. It is clear that this effect should be included in simulations in order to provide increased fidelity. The present method, however, is computationally intensive and thus inappropriate for real-time simulation. It can be used as a tool for building a modified dynamic inflow method which takes into account the ship ground effect.

The ship airwake effect has been shown to be quantitatively more important than the ship ground effect and somewhat localized. It cannot be even crudely approximated by a simple panel method and requires the availability of a ship airwake database in order to provide a realistic simulation.

Overall, the present work provided an insight into the relevant helicopter/ship aerodynamic interaction phenomena, and suggests additional parametric investigations, including simulation of approach flights where ship airwake turbulent components of velocity are included.

ACKNOWLEDGMENT

REFERENCES

1. Ferrier, B., and Semenza, J., "NATC Manned Flight Simulator VTOL Ship Motion Simulation and Application," 46th Annual Forum of the American Helicopter Society, Washington, DC, 1990.

2. Healey, J. Val., "The Prospects for Simulating the Helicopter/Ship Interface," *Naval Engineers Journal*, March 1987, pp. 45-63.

3. Hurst, D. W., and Newman, S. J., "Wind Tunnel Measurements of Ship Induced Turbulence and the Prediction of Helicopter Rotor Blade Response," *Vertica*, Vol. 12, No. 3, 1988, pp. 267-278.

4. Healey, J. Val., "Establishing a Database for Flight in the Wakes of Structures," *Journal of Aircraft*, Vol. 29, no. 4, July-August 1992, pp. 559-564.

5. Rhoades, M. M., and Healey, J. Val., "Flight Deck Aerodynamics of a Nonaviation Ship," *Journal of Aircraft*, Vol. 29, no. 4, July-August 1992, pp. 619-626.

6. Carico, D., Reddy, B., and Dimarzio, C., "Ship Airwake Measurements and Modeling Options for Rotorcraft Applications," In: Aircraft Ship Operations, AGARD CP-509, November 1991.

7. Arney, A. M., Blackwell, J., Erm, L. P., and Gilbert, N. E., "A Review of Australian Activity on Modelling the Helicopter/Ship Dynamic Interface," In: Aircraft Ship Operations, AGARD CP-509, November 1991.

8. Prasad, J. V. R., Mavris, D. N., and Schrage, D. P., "Ship Airwake Modeling and Simulation, Phase I — Methodology Development," Research Report submitted to Naval Air Warfare Center, School of Aerospace Engineering, Georgia Institute of Technology, Atlanta, August 1992.

9. Howlett, J. J., "UH-60A Black Hawk Engineering Simulation Program: Volume I — Mathematical Model," NASA CR-166309, 1981.

10. Stepniewski, W. Z. and Keys, C. N., *Rotary-Wing Aerodynamics*, Dover, 1984.

11. Mello, O. A. F., "Numerical Simulation of Helicopter / Ship Airwake Interactions," Research Report submitted to Naval Air Warfare Center, School of Aerospace Engineering, Georgia Institute of Technology, Atlanta, July 1993.

12. U.S. Department of the Army — Aeroflightdynamics Directorate, "2GCHAS Theory Manual," (Second Generation Comprehensive Helicopter Analysis System, Version 2.1), Vol. II, Chapter 5 – Airloads and Induced Velocity, Ames Research Center, Moffett Field, CA, July 1992.

13. Hess, J. L., and Smith, A. M. O., "Calculation of Potential Flow about Arbitrary Bodies," *Progress in Aeronautical Sciences*, Vol. 8. Edited by D. Küchemann. Pergamon Press, Oxford, England, 1967.

14. Westra, D. P., Sheppard, D. J., Jones, S. A., and Hettinger, L. J., "Simulator Design Features for Helicopter Shipboard Landing: II. Performance Experiments," Naval Training Systems Center, Orlando, FL, Report No. NTSC TR-87-041, July 1987.

APPENDIX 2

A SIMULATION MODEL OF SHIP GROUND EFFECT
FOR ROTORCRAFT / SHIP INTERACTION STUDY

Hong Zhang[*]   O.A.F.Mello[*]   J.V.R.Prasad[‡]   L.N.Sankar [†]   and   John D. Funk,Jr.[§]

School of Aerospace Engineering
Georgia Institute of Technology
Atlanta, GA

Aero Analysis Division
Naval Air Warfare Center Aircraft Division
Warminster, PA

Abstract

A simple ground effect model for rotorcraft / ship dynamic interactions, which is suitable for implementation in flight simulators for real-time simulation purposes, has been extracted from the analysis of the aerodynamic interaction results obtained from a computationally intensive method that incorporates a rigid rotor wake and a panel representation of the ship with corresponding image systems. It is found that the ground effect is very sensitive to the helicopter position with respect to the ship deck, as well as the height above the deck. The inflow gain matrix in dynamic inflow model is modified as a function of the position (x,y,z) relative to the deck. Numerical results for a SH-60 helicopter flying above the deck of a moving FFG-7 class frigate at the same speed as the ship are presented and discussed in this paper. Results show that the ground effect model works well all over the deck. The ground effect model integrated with the airwake model which has already been developed at Georgia Tech provides the basis for the real-time simulation study for rotorcraft/ship interactions.

1. Introduction

Modern helicopters must routinely operate under various adverse weather conditions. Helicopter landing on a moving ship deck behind the superstructure is hazardous[10], and yet up to today, little knowledge about the flow characteristics is available due to the time dependent uncertainty nature of the flow, as well as the complicated and sensitive flow field over the deck behind the superstructure. Because the lack of a suitable ship airwake model and the still unsolved rotorcraft / ship dynamic interaction problem, any realistic simulation of helicopter take-off and landing on a ship deck is still impractical. Also, in real time implementation, these models have to be computationally simple. A series of studies of these effects and models have been carried on at Georgia Tech [1,2] for the past few years, and a suitable ship airwake model and a systematic simulation method have already been developed. Moreover, a method to analyze helicopter/ship aerodynamic interactions has been formulated recently by Georgia Tech researchers[3]. It is found that the widely used traditional ground effect model, which basically introduces a factor to modify the uniform inflow of the helicopter rotor[8,9], is not accurate for a helicopter operating under a ship "ground effect".

A computationally intensive method, which combines a rigid rotor wake model and the well developed traditional potential flow theory, is formulated in Ref.(3) and the method is used here to generate the data base for the ground effect model identification. Our purpose in this paper, however, is to identify a simple ground effect model suitable for real-time simulation implementation.

2. Computational Fluid Dynamics (CFD) Model Used for Generating the Data Base

The ship "ground effect" is manifested by the changes of the flow field, so that the flow at the ship surface follows the motion of the ship surface. This effect is modeled by a panel representation of the ship surface, and the strength of the panel is determined by satisfying the boundary condition at the ship surface, i.e. there is no penetration of flow through the solid ship surface and/or ship deck. The velocity induced by the rotor wake on the ship surface is computed by using a rigid wake theory. The simulation of helicopter motion near the ship is carried out by the general helicopter simulation code GENHEL[8], which has been modified to incorporate a first-order dynamic inflow model[11]. By taking into account the induced velocity or upwash at the rotor disk due to the ship panel system into the blade-element analysis, the ground effect is coupled into the simulation code. Through changing the collective pitch and cyclic pitch, the helicopter is retrimmed at the same location with the consideration of the ground effect. The total inflow at the rotor disk is outputted as the rotor blade rotates azimuthally, and this forms the data base for later analysis.

3. Dynamic Inflow Model

A generalized dynamic inflow theory exists in the literature in which air mass passing through the rotor is treated as a dynamic system. The dynamic inflow theory [4,5,6,7] has found wide applications in flight dynamics and aeroelastic studies. Peter's dynamic inflow model [6] is used in this investigation for simplicity, i.e. the induced inflow is assumed to have the following variations:

$$\lambda(\bar{r},\bar{\psi}) = \lambda_0 + \lambda_s \frac{r}{R}\sin\psi + \lambda_c \frac{r}{R}\cos\psi \qquad (1)$$

where:

$\lambda_0, \lambda_s, \lambda_c$ are the uniform, lateral and longitudinal variations of the rotor inflow in tip path plane (tpp), respectively.

The dynamic inflow model is:

$$[M]\{\overset{\bullet}{\hat{\lambda}}\} + [\hat{L}]^{-1}\{\overline{\lambda}\} = \{\overline{C}\}_{aero} \qquad (2)$$

where

$$\lambda = (\lambda_0, \lambda_s, \lambda_c)^T$$
$$C = (CT, -C1, -C2)^T$$

$[M],[\hat{L}]$ are the apparent mass matrix and the inflow gain matrix and their explicit expressions for out-of-ground effect case can be found in Ref. [4]. CT is the thrust coefficient. C1,C2 are instantaneous aerodynamic rolling and pitching moment coefficients expressed in the tip path plane. Obviously, they are time dependent for unsteady flight.

The subscript "aero" denotes that only the aerodynamic contribution is considered and the inertial part is not included. The " • " denotes time derivative.

Due to the proximity of the rotor disk to the ship deck, the rotorcraft/ship interactions induce upwash at the rotor disk, thereby changing the total inflow and the inflow distribution over the whole rotor disk. Hence, it is not surprising that $[M]$ and $[\hat{L}]$ matrices are going to change due to the ground effect. Thus, the dynamic inflow model near the ground can be written as:

$$[M]_{ige}\{\overset{\bullet}{\hat{\lambda}}\}_{ige} + [\hat{L}]^{-1}_{ige}\{\overline{\lambda}\}_{ige} = \{\{\overline{C}\}_{aero}\}_{ige} \qquad (3)$$

where : $[M]_{ige}$, $[L]_{ige}$ are the apparent mass and the inflow gain matrices with ground effect.
Suppose

$$\{\lambda\}_{ige} = \begin{bmatrix} \alpha_1 & 0 & 0 \\ 0 & \beta_1 & 0 \\ 0 & 0 & \gamma_1 \end{bmatrix} \{\lambda\}_{oge} \qquad (4)$$

and

$$\{\overline{C}\}_{ige} = \begin{bmatrix} \alpha_2 & 0 & 0 \\ 0 & \beta_2 & 0 \\ 0 & 0 & \gamma_2 \end{bmatrix} \{\overline{C}\}_{oge} \qquad (5)$$

where:

$\alpha_i, \beta_i, \gamma_i \ (i = 1,2)$ are the correction factors to account for ground effect to the inflow and the forcing functions,

which are functions of the helicopter position (x,y,z) relative to the deck.

Thus, for the steady case, i.e., trimmed flight condition,

$$[\hat{L}]_{ige} = \begin{bmatrix} \alpha_1/\alpha_2 & \alpha_1/\beta_2 & \alpha_1/\gamma_2 \\ \beta_1/\alpha_2 & \beta_1/\beta_2 & \beta_1/\gamma_2 \\ \gamma_1/\alpha_2 & \gamma_1/\beta_2 & \gamma_1/\gamma_2 \end{bmatrix} [\hat{L}]_{oge} \qquad (6)$$

All six factors $\{\alpha_1, \beta_1, \gamma_1, \alpha_2, \beta_2, \gamma_2\}$ can be obtained by conventional identification methods.
For trimmed flight (steady case), we have:

$$\{\overline{\lambda}\} = [\hat{L}]\{\overline{C}\}_{aero} \qquad (7)$$

Thus, for trimmed hovering with respect to the deck of the moving ship, since the forcing functions (CT,C1,C2) are approximately the same for out-of-ground case and in-ground case, Eq. (6) reduces to:

$$\{\hat{L}\}_{ige} = \begin{bmatrix} \alpha_1 & 0 & 0 \\ 0 & \beta_1 & 0 \\ 0 & 0 & \gamma_1 \end{bmatrix} \{\hat{L}\}_{oge} \qquad (8)$$

4. Identification Approach

For illustration purpose, the SH-60 Seahawk helicopter flying at 15kts above the deck of a FFG-7 class frigate, which is moving at the same velocity as the helicopter, is used in this investigation. To capture the ground effect, the rotorcraft/ship interactions are computed using the CFD code at all the grid points over the ship deck as shown in Figure 1(a) at eight heights ranging from 0.5R to 3R for each grid point (Figure 1(b))
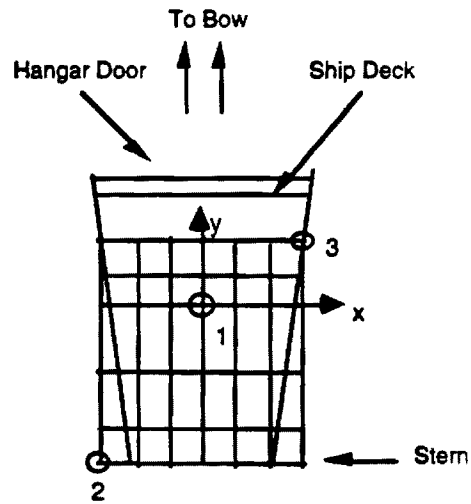

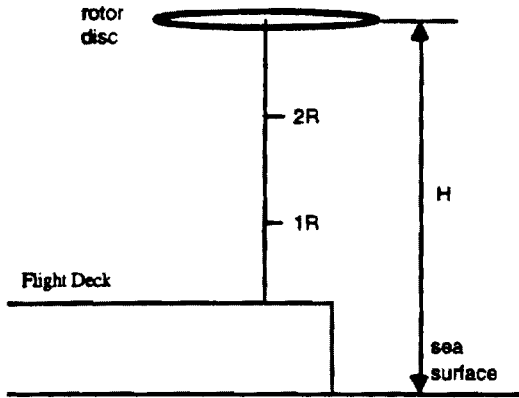Figure 1(a): Positioning of helicopter above
ship deck (top view)

Figure 1(b): Helicopter Relative Position

It is recognized that the ground effect and the ship airwake effect are actually coupled when the helicopter is flying near the deck. However, only the ground effect part is considered in this study.

Figures 2(a) and 2(b) show how the nondimensional upwash at 80% radial station changes in one revolution above the center of the deck (location 1 in Figure 1(a)) and at the lower left corner of the deck (location 2 in Figure 1(a)) for different values of height above the deck.

It can be seen from Figure 2(a) that the upwash is almost constant at the fore part of the rotor for a given height (azimuth angle between 90 and 270 degrees), whereas at the rear part of the rotor (azimuth angle form 0 to 90, and 270 to 360 degrees), the upwash changes significantly. Also, we see that the effect of the height on upwash is different at different azimuth angles, hence it is not accurate to model this effect by using a simple constant factor. Because of the presence of the hanger, the rotor wake hits the deck differently at different locations.

For the case of the rotor hovering above the lower left corner of the deck, the upwash is much higher at advancing side and much lower at retreating side (see Fig. 2(b)). In order to incorporate the upwash in the dynamic inflow model, harmonic analysis of the upwash is carried out in order to extract the uniform and lateral and longitudinal variations due to the contribution of the upwash from the ground effect. It is seen from this analysis that terms up to second harmonic are required in order to account for the effect of ship deck on the rotor inflow variation.

$$\Delta w = -\Delta \lambda_0 - \Delta \lambda_s \frac{r}{R} \sin \psi - \Delta \lambda_c \frac{r}{R} \cos \psi$$

$$- \Delta \lambda_{2s} \frac{r}{R} \sin(2\psi) - \Delta \lambda_{2c} \frac{r}{R} \cos(2\psi) \quad (9)$$
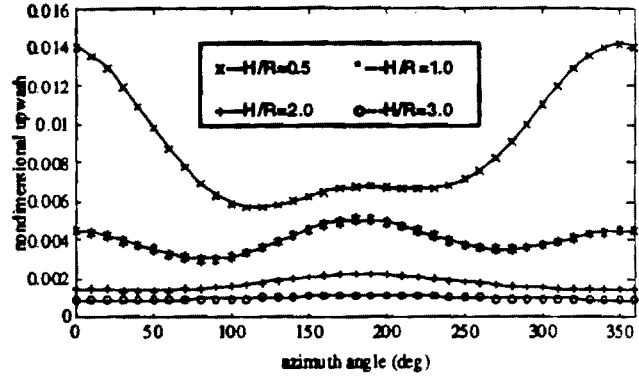
where

Figure 2(a): Effect of height on upwash at rotor disk at the center of the deck
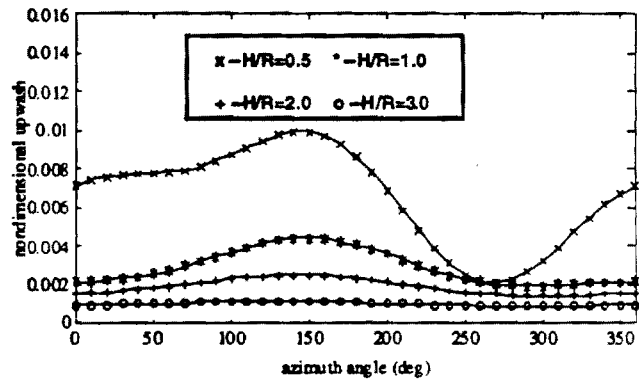

Figure 2(b): Effect of height on upwash at the rotor at the lower left corner of the deck

$\Delta \lambda_0$ is the upwash contribution to the uniform inflow

$\Delta \lambda_s$ is the lateral inflow changes due to the ground effect

$\Delta \lambda_c$ is the longitudinal inflow variation because of the ground presence

$\Delta \lambda_{2s}$ is the 2nd lateral inflow change

$\Delta \lambda_{2c}$ is the 2nd longitudinal inflow change

The analysis is carried out for different heights from 0.5 R to 3 R above the deck.

Figure 3 gives the effect of the height on the uniform inflow changes for location 1 (center of the deck, "*" in Fig.3--5) and for location 2 (left corner at the stern, "o" in Fig.3--5). The magnitude of total uniform inflow increases as the height increases. This is quite reasonable, because the ground cushion effect gets less and less as the rotor moves away from the deck, hence the upwash gets less and less. We see that at the deck center, the uniform inflow undergoes a maximum of 14% change due to "ground" effect.

Figures 4(a) and 4(b) give the effect of height on the first harmonic lateral inflow λ_s and first harmonic longitudinal inflow component λ_c
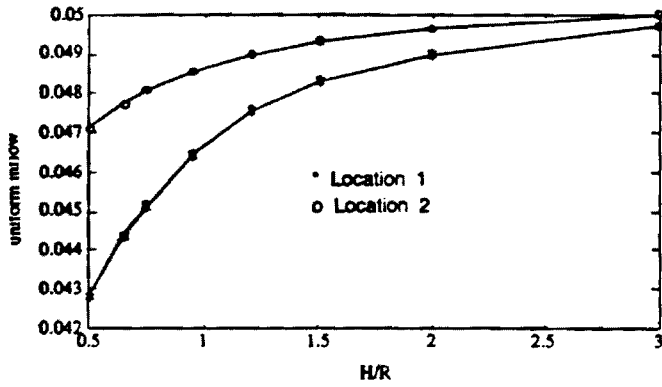
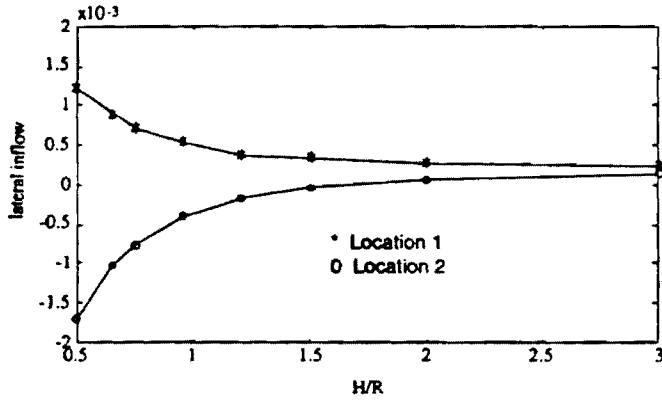Figure 3: Effect of height on uniform inflow

Figure 4(a) : Effect of height on lateral inflow
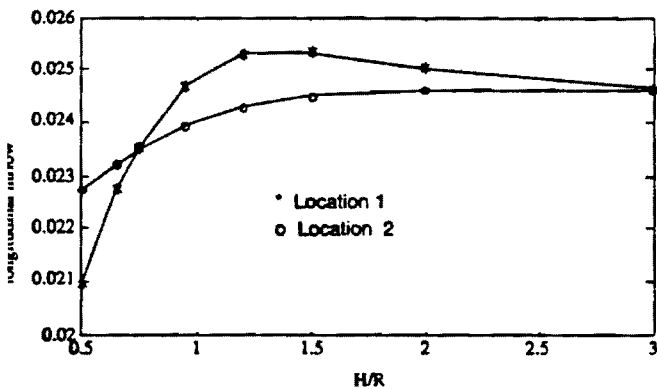(First harmonic term)

Figure 4(b): Effect of height on longitudinal inflow
(First harmonic term)

It is seen from Fig 4 that the longitudinal inflow change is not a linear function of height.

Figures 5(a) and 5(b) are the effect of height on the 2nd inflow terms λ_{2s} , λ_{2c}. Still, the ground effect gets less important as the distance between the helicopter and the

deck gets larger. Also, the lateral component in the upwash is smaller than the longitudinal component.

From Figs 3,4 and 5, it can be seen that the ground effect is not a linear function of the height, and it is sensitive to the location of the rotor hub over the deck.
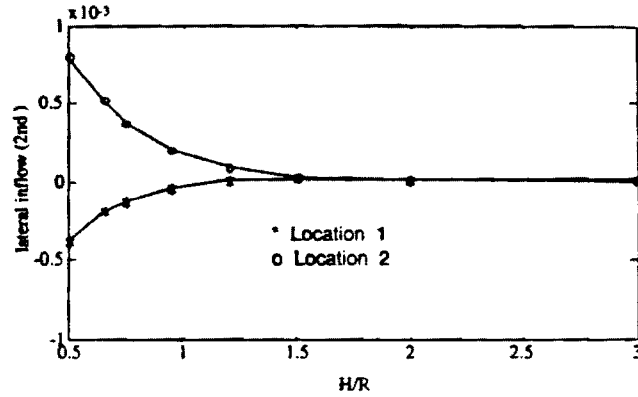

Figure 5(a): Effect of height on lateral inflow
(2nd harmonic term)
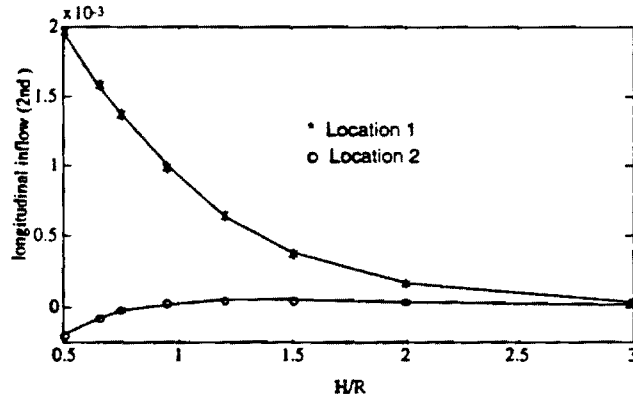
Figure 5(b): Effect of height on longitudinal inflow
(2nd harmonic term)

Several models are tried to represent these changes. By comparison of the **Pearson** correlation coefficient, the following model is seen to capture the variation with height:

$$\{\lambda_i\} = \{\lambda_i\}_{ref} \ [a + \frac{b}{h} + \frac{c}{h^2} + \frac{d}{h^3}] \qquad (10)$$

where :
a,b,c,d are constants for a given location w.r.t. the deck, h is the nondimensional (w.r.t. rotor radius R) height, and λ_{ref} is the corresponding value of the component out of ground effect.

Thus from (5) and (10),

$$\left\{ \begin{array}{c} \alpha_1 \\ \beta_1 \\ \gamma_1 \end{array} \right\} \Rightarrow a + \frac{b}{h} + \frac{c}{h^2} + \frac{d}{h^3} \qquad (11)$$
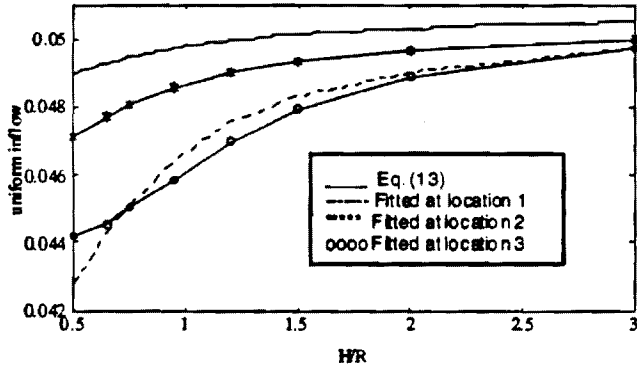
Cheeseman and Bennett [9] derived an expression for the upwash at the rotor disk due to the ground:

$$\Delta w = \frac{\lambda_{0ref}}{16h^2} \qquad (12)$$

i.e.

$$\lambda_0 = (1. - \frac{1}{16h^2})\lambda_{0ref} \qquad (13)$$

Figure 6 shows the comparison of the uniform inflow predicted by the simple model Eq.(13) and the fitted model of Eq. (10) at several locations.

We see that the Cheeseman model is not accurate enough to capture the ship ground effect. First the ground effect is location dependent, and second it does not follow the h^{-2} law . Hence the ship ground effect model has to incorporate a function of location x and y, as well as the height.

5. Spline Fit

Having taken care of the effect of the height, we now move to the modeling of the location effect. Based on the data base, it is found that we can not use a simple function for f(x,y) to fit these data. Because spline fit has advantages of passing through every grid point, and yet it preserves the nice continuous property (up to 2nd derivatives), we use a two dimensional spline-fit to model the ground effect, i.e. a,b,c,d will be spline functions of x and y.

Suppose we have a set of data on the grid of X and Y as:

$$X=\{X_i\}, \quad i=1,2,......m+kx$$
$$Y=\{Y_j\}, \quad j=1,2,...... n+ky$$
$$F=\{ f(x_i,y_j)\}$$

where: kx is the order of the spline in x direction, ky is the order of the spline in y direction. For cubic spline, the order is 4. For quadratic spline, the order is 3.

Let:

$$qx = m + kx$$
$$qy = n + ky$$

$N_{kx,i}(X,x)$ denotes the normalized B-spline of order kx in x direction with support $[X_{i-kx},X_i]$

$N_{ky,j}(Y,y)$ denotes the normalized B-spline of order ky in y direction with support $[Y_{j-ky},Y_j]$

Then any bivariate spline S(x,y) of order kx in x, and ky in y, has the following representation:

$$S(x,y) = \sum_{i=1}^{qx} \sum_{j=1}^{qy} C_{i,j} N_{kx,i}(X,x) N_{ky,j}(Y,y) \qquad (14)$$

With the help of **Mathematica** [12], the coefficients C_{ij} are obtained for cubic spline fit. That is kx=ky=4.

Finally the total inflow with ground effect is modeled as:

$$\lambda = \lambda_0 + \frac{r}{R}(\lambda_s \sin(\psi) + \lambda_c \cos(\psi) + $$
$$\lambda_{2s} \sin(2\psi) + \lambda_{2c} \cos(2\psi)) \qquad (15)$$

and

$$\{\lambda_i\} = \{\lambda_i\}_{ref}[a(x,y) + \frac{b(x,y)}{h} + \frac{c(x,y)}{h^2} + \frac{d(x,y)}{h^3}] \qquad (16)$$

where i may be $0,s,c,2s,2c$.

For illustration purpose, the following is the spline fitted result for the uniform inflow:

$$\lambda_0 = 0.994 - 0.0448x - 0.2993x^2 - 0.1752x^3 - 0.0355xy$$
$$+ 0.036x^2y + 0.040x^3y + 0.027xy^2 + 0.236x^2y^2$$
$$+ 0.14x^3y^2 + 0.0177y^3 + 0.069xy^3 - 0.066x^2y^3$$
$$- 0.074x^3y^3$$
$$+ (0.011 + 0.486x + 2.334x^2 + 1.3x^3 + 0.026y$$
$$+ 0.269xy - 0.298x^2y - 0.325x^3y - 0.0625y^2$$
$$- 0.2656xy^2 - 1.8x^2y^2 - 1.05x^3y^2 - 0.1358y^3$$
$$- 0.53xy^3 + 0.55x^2y^3 + 0.594x^3y^3) /h$$
$$+ (-0.2255 - 1.55x - 5.587x^2 - 3.02x^3 - 0.0389y$$
$$- 0.6457xy + 0.7674x^2y + 0.815x^3y + 0.077y^2$$
$$+ 0.76xy^2 + 4.25x^2y^2 + 2.42x^3y^2 + 0.327y^3$$
$$+ 1.28xy^3 - 1.437x^2y^3 - 1.5x^3y^3) /h^2$$
$$+(-0.05999 + 1.21x + 3.9x^2 + 2.05x^3 + 0.01557y$$
$$+ 0.4987xy - 0.61x^2y - 0.639x^3y + 0.183y^2$$
$$- 0.534xy^2 - 3.x^2y^2 - 1.685x^3y^2 - 0.2448y^3$$
$$- 0.9727xy^3 + 1.157x^2y^3 + 1.17886x^3y^3) /h^3$$

$$(17)$$

The computation with the above formula is quite fast when compared to the CFD code used to build the database. For comparison, CFD code takes about 30 minutes of CPU time in HP Apollo 700 Workstation to obtain a converged solution for a helicopter flying at one single height and single (x,y) location. Whereas using the above formula, the computation is carried out in a fraction of a second. Hence the formula is very useful for real-time simulation purposes. Figure 7 shows the variation of the uniform inflow over the whole deck at height h=0.75.

Figures 8 and 9 display the variation of the harmonics of the inflow at h=0.75. It can be seen that the total inflow mainly consists of the uniform inflow and the longitudinal variation. This is from the fact that the reference flight is forward flight.
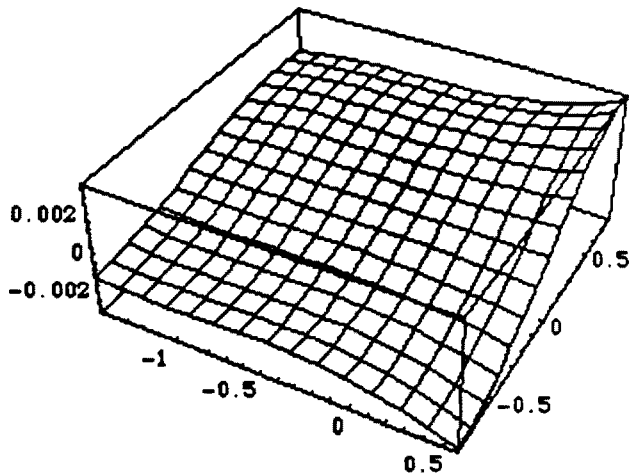
Figure 9: distribution of the lateral inflow over the deck

Figures 10(a) and 10(b) compare the results from the CFD code and from the formula at location x=-7.5/R, y=-5.5/R, h=0.75 and x=-25/R,y=15/R, h=1.75. We see that the fitted formula computes the inflow variation quite well.
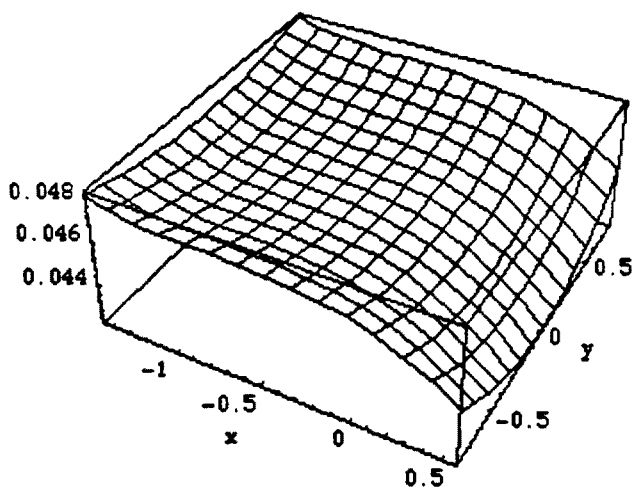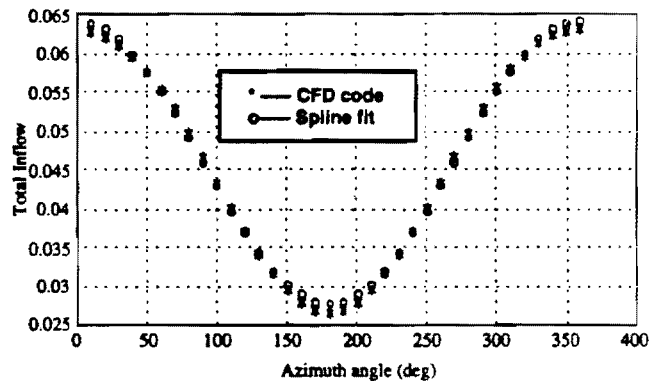
Figure 7: distribution of the uniform inflow over the deck

Figure 10 (a): comparison of the total inflow from CFD code and Spline fit formula at h=0.75
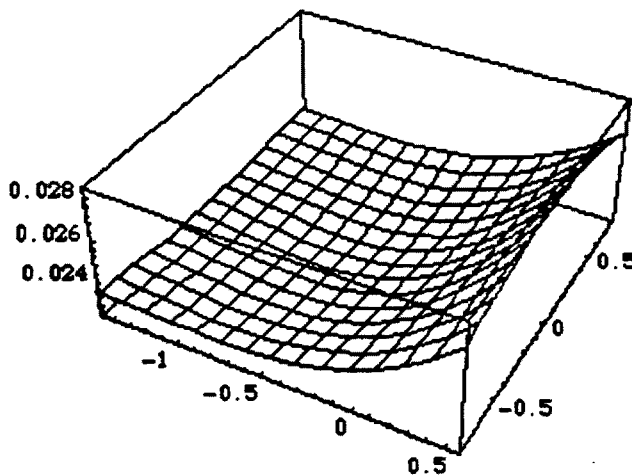
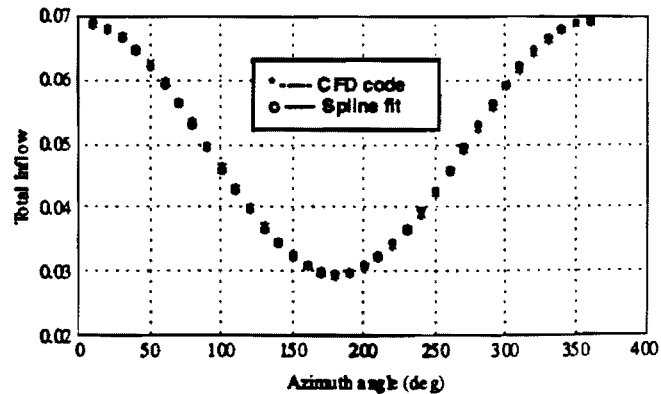Figure 8: distribution of the longitudinal inflow over the deck

Figure 10 (b): comparison of the total inflow from CFD code and Spline fit formula at h=1.75

6. Conclusions

A ground effect model for rotorcraft/ship dynamic interface that is suitable for real time simulation purposes is developed in this paper. The gain matrix in the dynamic inflow model is identified as a function of the location of the rotor with respect to the ship deck, as well as the height of the rotor above the deck. However, the ship ground effect model developed in this study is applicable for trimmed flight above the deck. Further work is needed to capture the unsteady effects due to the rolling and/or pitching of the ship deck.

References

1.Prasad, J.V.R., Mavris, D.N., and Schrage, D.P., "Ship Airwake Modeling and Simulation, Phase I --- Methodology Development", Research Report submitted to Naval Air Warfare Center, School of Aerospace Engineering, Georgia Institute of Technology, Atlanta, Aug. 1992

2.Zhang, H., Prasad, J.V.R., and Mavris, D.N., "Ship Airwake Effects on Helicopter Rotor Aerodynamics", AIAA 94-3509, Arizona, August, 1994

3.Mello, O.A.F., Prasad, J.V.R., Sankar, L.N., and Tseng, W., "Analysis of Helicopter/Ship Aerodynamic Interactions," AHS Aeromechanics Specialists Conference, San Francisco, California, Jan. 1994.

4.Gaonkar, G.H., and Peters, D.A., "Review of Dynamic Inflow Modeling for Rotorcraft Flight Dynamics," Vertica, Vol. 12, No. 3, pp. 213-242, 1988.

5.Pitt, D.M., and Peters, D.A., "Theoretical Prediction of Dynamic Inflow Derivatives", Sixth European Rotorcraft and Powered Lift Aircraft Forum, Bristol, England, Sept. 1980

6.Peters, D.A., and HaQuang, N., "Dynamic Inflow for Practical Applications" J. of AHS, Oct. 1988.

7.He, Changjian, and Lewis, W.D., "A Parametric Study of Real Time Mathematical Modeling Incorporating Dynamic Wake and Elastic Blades", 48th Annual Forum of the AHS, Washington, DC, June 1992.

8.Howlett, J.J., "UH-60A Black Hawk Engineering Simulation Program: Volume I -- Mathematical Model", NASA CR-166309, 1981.

9.Cheeseman, I.C. and Bennett, W.E., "The Effect of the Ground on a Helicopter Rotor in Forward Flight", ARC R&M No.3021, Sept. 1955.

10. Healey, J. Val., "Prospects for Simulating the Helicopter/Ship Interface," Naval Engineers Journal, Vol. 99, No. 2, March 1987, pp. 45-63.

11. Mello, O. A. F., Numerical Simulation of Helicopter/Ship Aerodynamic Interactions," Research Report submitted to Naval Air Warfare Center, School of Aerospace Engineering, Georgia Institute of Technology, Atlanta, July 1993.

12. Wolfram, S., Mathematica: A System for Doing Mathematics by Computer, Addison-Wesley, Redwood City, Calif., 1988.

APPENDIX 3

GROUND EFFECT SIMULATION MODEL
FOR ROTORCRAFT/SHIP INTERACTION STUDY

Hong Zhang [*] J.V.R. Prasad[†] L.N. Sankar[‡]
School of Aerospace Engineering
Georgia Institute of Technology
Atlanta, GA 30332, USA

O.A.F. Mello[§]
Centro Técnico Aerocspacial
Instituto de Aeronáutica e Espaco
São José dos Campos-SP, BRAZIL

John D. Funk, Jr.[¶]
Aircraft Division
Naval Air Warfare Center
Warminster, PA, USA

Abstract

In this paper, a real time simulation model of ship ground effect for rotorcraft/ship interactions is developed by combining computational fluid dynamics (CFD) analysis and finite state representation of rotor inflow. For CFD analysis, the ship is modeled by using a source panel representation and the rotor wake is modeled as rigid with prescribed geometry but unknown vorticity distribution. The sea surface is modeled by placing an image rotor wake and an image ship panel system below the sea surface. The CFD model is then combined with the batch version of a generic helicopter flight simulation program. Using trim solutions from the simulation program, the ship ground effects on rotor inflow for cases of helicopter hovering with respect to ship deck are identified and analyzed. With a finite state representation of rotor inflow, a real time simulation model of ship ground effect is developed using results from the CFD analysis.

1. Background

Due to complex flow interactions between the air flow surrounding the ship deck and rotor wake, the pilot workload during shipboard landing and take-off of a helicopter is significantly increased [1]. Also, When a helicopter is flying close to a ship deck, the rotor wake is modified due to the presence of ship deck, superstructure and sea surface [2-4]. An alternative, to extensive and time-consuming testing at sea for establishing safe operating envelopes for helicopter shipboard operations, is simulation. A prerequisite to simulation approach is the development of simulation models of ship airwake and ship ground effect. This paper addresses the development of a simulation model of ship ground effect model while a companion paper [5] addresses the development of a simulation model of ship airwake. The organization of the paper is as follows: First, the methodology used for the development of a real-time ship ground effect simulation

model is described. Next, a detailed description of the CFD modeling used in this methodology is presented followed by parametric investigations of the CFD model. Then a brief description of the real-time simulation model which is obtained by modifying the gain matrix of an existing dynamic inflow model is given and results are presented to illustrate how the real-time simulation model captures the ship ground effect for different rotor heights above deck and at various forward speeds.

2. Methodology for Developing Ship Ground Effect Simulation Models

The methodology used for developing ship ground effect simulation models is given in Fig. 1. First, a comprehensive computational fluid dynamic model that takes into account interactions between rotor wake and ship deck, superstructure and sea surface is developed. The CFD model is then combined with a comprehensive non-real time helicopter simulation model and rotor inflow distribution for cases of helicopter trimmed at different positions (see Fig. 2) and at different heights (see Fig. 3) with different values of ship speed are obtained. Then a harmonic analysis of inflow distribution for each of the cases is carried out. Using results from the harmonic analysis, the gain matrix of the dynamic inflow model is modified by matching the inflow distribution predicted by the dynamic inflow model with CFD results.
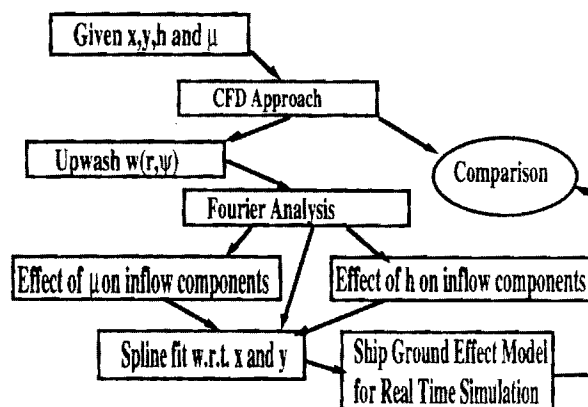

Figure 1. Methodology for Developing Ship Ground Effect Models

---

* Graduate Research Assistant
† Associate Professor, Member AIAA
‡ Professor, Member AIAA
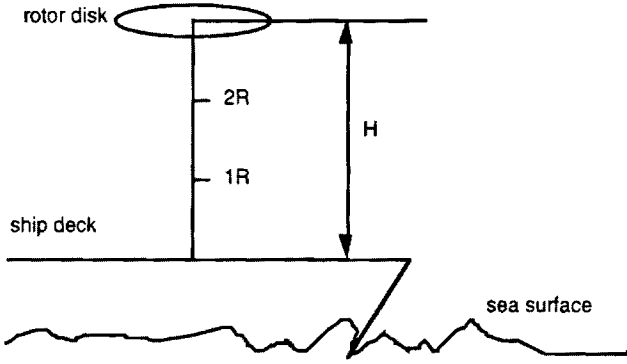§ Captain, Brazil Air Force
¶ Aerospace Engineer
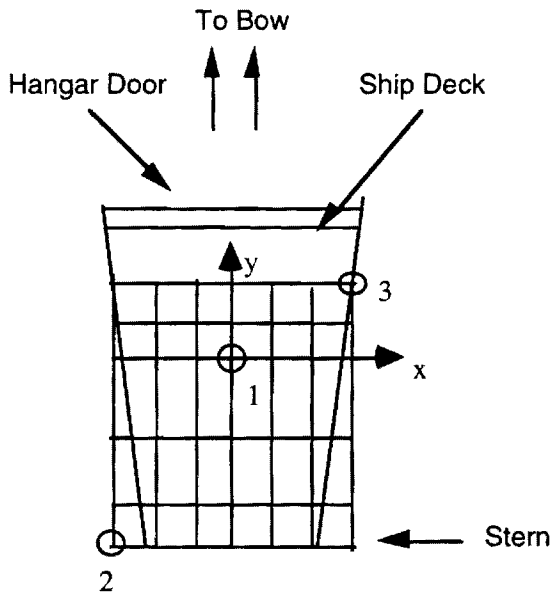
Figure 2. Helicopter Relative Position

Figure 3. Positioning of Helicopter above
Ship Deck (top view)

3. CFD Modeling

3.1 Ship Formulation

The ship surface is approximately represented by plane source panels with constant distributed strength. The strengths of the sources are determined by enforcing the non-penetration condition at the centroid of each panel. The normal component of the ship's motion and the normal component of the downwash induced by the rotor are taken into account in this formulation. The details of the source panel method can be found in Ref. 6 and therefore will not be repeated here. This formulation results in a linear system of equations to be solved for the ship panel source strengths σ:

$$[A]\{\sigma\} = [B] \tag{1}$$

where $[A]$ is the matrix of influence coefficients, $\{\sigma\}$ is the vector of unknown source strengths and $[B]$ is the RHS including the normal component of the velocities on the ship surface due to the free-stream and due to the rotor and its wake. The resulting source panel strengths are used to compute the velocities induced by the ship source panel system at the rotor disk.

3.2 Rotor Wake Formulation

A rigid wake model is used to compute the induced velocity due to the rotor and its wake on the ship and the vorticity distribution is computed from the blade section lift. In this study, the following assumptions are made:

(a) Blade flapping angles is small and high harmonic variation of blade flapping angle are negligible

(b) The rotor blade is modeled by a lifting line of bound vorticity, which is related to the blade section lift by Kutta-Joukowski's theorem.

(c) A classical skewed helical wake with a limited contraction is used, the wake is assumed to become flat near the ship deck as shown in Fig. 4.

(d) The wake is divided into a "near" wake, composed of trailing and shed vortices and a "far" wake composed of trailing tip vortices only. The strength of the far wake tip vortex is assumed to be equal to the maximum bound vorticity at the azimuthal location where the vortex filament leaves the blade.

(e) The rotor wake is convected downstream with a velocity which is equal to the vector sum of the free stream velocity and the averaged (momentum theory value) induced velocity over the disk.

3.2.1 Bound Vortices

The blade bound vorticity distribution is obtained through an iterative process from the blade section lift. Let the blade bound vorticity be $\Gamma_{b_{ij}} = \Gamma_b(r_i, \psi_j)$. From Kutta-Joukowski theorem:

$$\ell_{ij} = \rho V_{ij} \Gamma_{ij} = \rho(\Omega R)(\bar{r}_i + \mu \sin \psi_j)\Gamma_{b_{ij}} \tag{2}$$

i.e.

$$\Gamma_{b_{ij}} = \frac{\ell_{ij}}{\rho(\Omega R)(\bar{r}_i + \mu \sin \psi_j)} \tag{3}$$

From the computed bound vorticity distribution, the velocity induced by the blade bound vortices can be obtained by applying the Biot-Savart law.

3.2.2 Near Wake

The near wake is assumed to be composed of trailing and shed vortices, with strengths given by the radial and azimuth-wise variations of the bound vorticity respectively, at the azimuth location where the vortex filament leaves the blade. Let us first consider an element of a trailing vortex filament of length $r_i \Delta v$, which leaves the blade at the radial location r_i, and is located at a wake age v_k. This element had left the blade when it was at an azimuth

2

location $\psi_j - v_k$, with ψ_j being the current azimuth location of the blade. Therefor, the vorticity of the element is given by $\Gamma_t(\bar{r}_i, \psi_j - v_k)\bar{r}_i \Delta v$, where

$$\Gamma_{t_{ijk}} = \Gamma_t(\bar{r}_i, \psi_j - v_k) = \frac{\partial \Gamma_b}{\partial \bar{r}} \qquad (4)$$

i.e.

$$\Gamma_{t_{ijk}} \approx \frac{\Gamma_b(\bar{r}_i, \psi_j - v_k) - \Gamma_b(\bar{r}_{i-1}, \psi_j - v_k)}{\bar{r}_i - \bar{r}_{i-1}} \qquad (5)$$

The velocity induced by the entire filament at a point is given by integration of elementary induced velocities obtained from the Biot-Savart law along the near wake only.

Now let us consider an element of a shed vortex filament of length Δr_i, which leaves the blade at the radial location r_i, and is located at a wake age v_k. This element had left the blade when it was at an azimuth location $\psi_j - v_k$, with ψ_j being the current azimuth location of the blade. Therefore, the vorticity of the element is given by $\Gamma_s(\bar{r}_i, \psi_j - v_k)$, where $\Gamma_s(\bar{r}_i, \psi_j - v_k)\Delta r_i$ is the shed vortex vorticity, equal to the azimuthal variation of Γ_b:

$$\Gamma_{s_{ijk}} = \Gamma_s(\bar{r}_i, \psi_j - v_k) = \frac{\partial \Gamma_b}{\partial \psi} \qquad (6)$$

$$\Gamma_{s_{ijk}} \approx \frac{\Gamma_b(\bar{r}_i, \psi_j - v_k) - \Gamma_b(\bar{r}_i, \psi_{j-1} - v_k)}{\Delta \psi} \qquad (7)$$

Also, the velocity induced by the entire shed vortex system at a point is given by radial integration of the elementary induced velocities obtained from the Biot-Savart law along the "near" wake.

3.2.3 Far wake

The far wake is assumed to be only composed of trailing tip vortices, with strength equal to the maximum bound vorticity at the azimuth location where the vortex filament leaves the blade. Considering an element of wake filament of length $r_{tv}\Delta v$ (where r_{tv} corresponds to the radial location where the tip vortex has rolled up) and at a wake age v_k. This element has left the blade when it was at an azimuth location $\psi_j - v_k, \psi_j$ being the current azimuth location of the blade. Therefore, the vorticity of the element is given by $\Gamma_{T_{jk}} r_{tv}\Delta v = \Gamma_T(\psi_j - v_k)r_{tv}\Delta v$, where $\Gamma_T(\psi_j - v_k)$ is the strength of the trailing tip vortex equal to the radial maximum of Γ_b:

$$\Gamma_{T_{jk}} = \Gamma_T(\psi_j - v_k) = \max_i (\Gamma_b(r_i, \psi_j - v_k)) \qquad (8)$$

3.2.4 Vortex Core Model

A Rankine vortex core model [7] with radius of one tenth (1/10) of the blade chord is used. This model is applied by scaling the induced velocity due to the elementary vortex filament by the square of the ratio between the distance to the filament and the core radius,

whenever the point where the induced velocity is being calculated lies within the vortex core. The geometry of the far wake is modified by making it flat and parallel to the ship deck with assumed clearance between the wake and the deck (see Fig. 4).
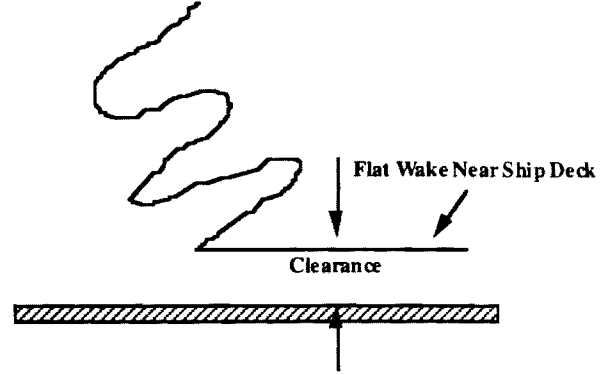

Figure 4. Modified Wake Geometry

In order to determine the number of rotor revolutions and clearance between the wake and the ship deck, the rotor wake model is combined with a generic helicopter simulation package [8]. Assuming a flat ground, the number of rotor revolutions in the wake geometry and wake clearance are adjusted by matching the rotor power required from analysis with experimental results. Figure 5 shows the effect of ground clearance on the rotor power required, whereas Fig. 6 illustrates the effect of number of revolutions in the wake geometry. It can be seen from Fig. 5, that the wake clearance has negligible effect on the rotor power. However, from Fig. 6, it is clear that the number of revolutions in the wake geometry has significant effect on rotor power. Also, from Fig. 6, it is seen that roughly 10 rotor revolutions of wake is needed in order to match with experimental data for the hover case. However, the results are less sensitive to number of revolutions for forward flight cases. It is felt that the value of 10 rotor revolution of wake geometry arrived at for the hover case is rather ad hoc as this value will be different for different heights of the rotor above the ground. Also, it is felt that a detailed investigation using , possibly, a free wake analysis is required to determine the wake geometry for the hover case. Hence, only forward flight cases are considered in the subsequent analysis.

4. Parametric Investigation

4.1 Effect of Locations

For illustration purpose, the SH-60 helicopter flying at 15kt above the deck of a FFG-7 class frigate, which is moving at the same velocity as the helicopter, is used in this investigation. The simulation of helicopter motion near the ship is carried out using the general helicopter simulation code [8]. By taking into account the induced velocity or upwash at the rotor disk due to the ship panel system into

3

the blade-element analysis, the ground effect is coupled into the simulation code. Through changing the collective pitch and cyclic pitch, the helicopter is retrimmed at the same location with the consideration of the ground effect. Using the coupled ship ground effect CFD model and the generic flight simulation package, the helicopter is trimmed at different locations and different heights above the deck.
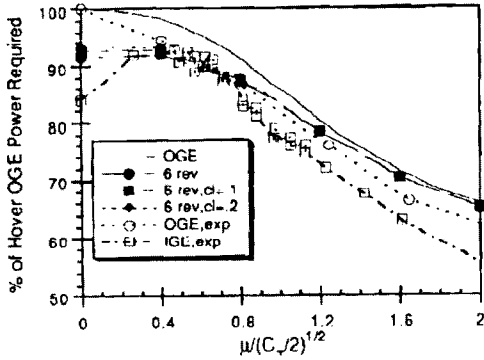

Figure 5. Clearance Effect on Power
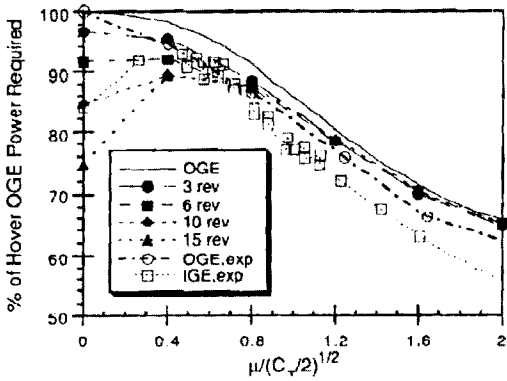
Figure 6. Effect of Number of Revolutions

Figure 7 shows the nondimensional upwash at 0.8R blade station for the rotor positioned at various heights above the center of the deck. It can be seen that the upwash is symmetric about the flight direction. The variation of the nondimensional upwash at the rotor at 0.8R blade station is shown in Fig. 8 for different heights of rotor from the ship deck for the helicopter above the lower left corner of the deck. It is seen from Fig. 8 that with an increase in rotor height above the deck, the ship ground effect diminishes. Also, the ship ground effect results in an increase in upwash on the advancing side of the rotor indicating, as one would expect, a "partial" ship ground effect.
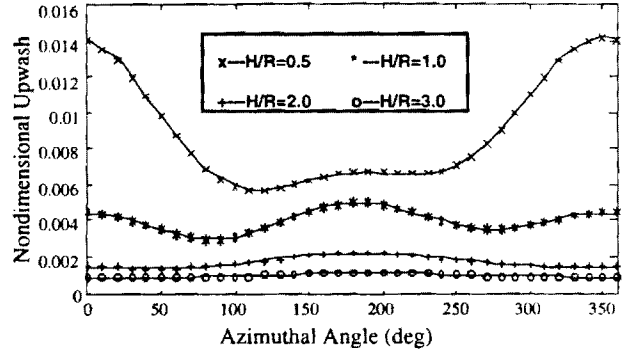
Figure 7. Effect of Height on Upwash at Rotor
Disk at the Center of the Deck
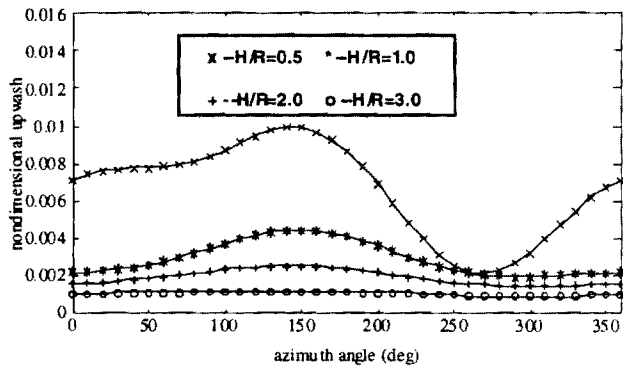
Figure 8. Effect of Height on Upwash at
Lower Left Corner of the Deck

4.2 Effect of Advance Ratio

To study the advance ratio effect on the inflow distribution over the rotor disk when flying near the ship deck with the ship in motion, the helicopter is trimmed at 1.2 R above the ship deck at various speeds ranging from 10kt to 80kt. Figure 9 compares upwash due to the ship deck between the cases of helicopter flying at 15kt and 45kt
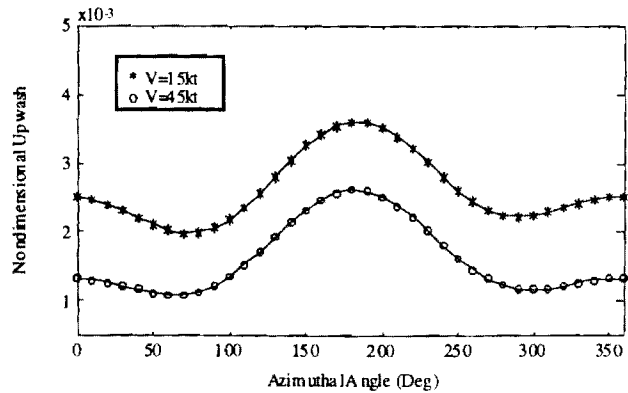
Figure 9. Upwash at Different Advance Ratio

4

cases. As expected, Fig. 9 shows that the upwash decreases as the helicopter speed is increased.

4. 3 Harmonic Analysis of the Inflow

Harmonic analysis is carried out for the upwash at various locations and advance ratios. It is found that up to second harmonic terms are needed to match the upwash from CFD results, i.e.:

$$\Delta w = -\Delta\lambda_0 - \Delta\lambda_s \frac{r}{R}\sin\psi - \Delta\lambda_c \frac{r}{R}\cos\psi$$
$$- \Delta\lambda_{2s}\frac{r}{R}\sin(2\psi) - \Delta\lambda_{2c}\frac{r}{R}\cos(2\psi) \tag{9}$$

where

$\Delta\lambda_0$ is the upwash contribution to the uniform inflow

$\Delta\lambda_s$ is the lateral inflow changes due to the ground effect

$\Delta\lambda_c$ is the longitudinal inflow variation because of the ground presence

$\Delta\lambda_{2s}$ is the 2nd lateral inflow change

$\Delta\lambda_{2c}$ is the 2nd longitudinal inflow change

Thus, the inflow in ship ground effect can be modeled as,

$$(\lambda)_{ige} = (\lambda)_{oge} - \Delta w \tag{10}$$

Figure 10 shows how the rotor height above the ship deck influences the uniform inflow at the rotor at two different locations. It is seen that the uniform inflow gets smaller when the rotor height above the ship deck increases, which is as expected. Figure 11 shows how the uniform inflow changes as the advance ratio varies. A nonzero value of advance ratio represents the case of the helicopter hovering with respect to the ship deck while the ship is in motion. The advance ratio effect on longitudinal inflow component is shown in Fig. 12. It is clear from Figs. 11 and 12 that the ship ground effect with advance ratio is not the same on average and the harmonic components. While the average component of inflow decreases with an increase of advance ratio, the longitudinal component of inflow first increases and then decreases as the advance ratio is increased.
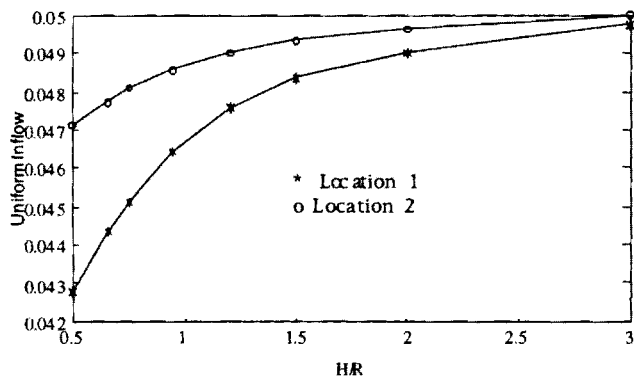
Figure 10. Effect of Height on Uniform Inflow Component
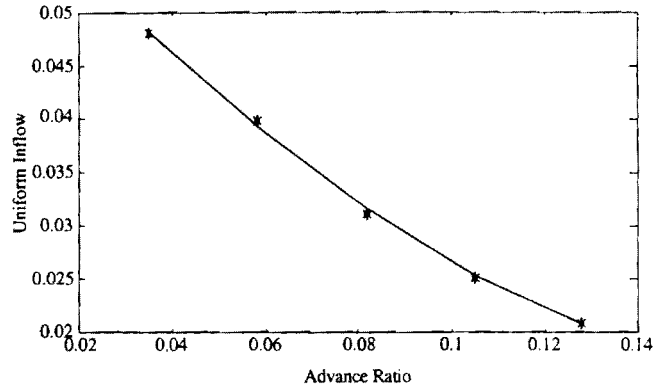
Figure 11: Effect of Advance Ratio on Uniform Inflow Component
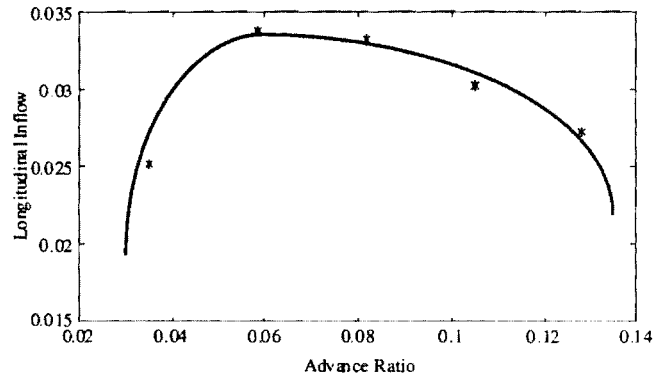
Figure 12. Effect of Advance Ratio on Longitudinal Inflow Component

5. Real Time Ship Ground Effect Model

As most of the current day flight simulation programs include a dynamic inflow representation for rotor inflow in order to account for the time-varying and distributed nature of inflow over the rotor disk, it is felt that a real time ship ground effect model can be obtained by appropriately modifying the parameters in the dynamic inflow model. The dynamic inflow model can be written as [9]:

$$[M]\{\dot{\bar{\lambda}}\} + [\hat{L}]^{-1}\{\bar{\lambda}\} = \{\bar{C}\}_{aero} \tag{11}$$

where

$$\bar{\lambda} = (\lambda_0, \lambda_s, \lambda_c)^T$$
$$C = (CT, -C1, -C2)^T$$

$[M], [\hat{L}]$ are the apparent mass matrix and the inflow gain matrix and their explicit expressions for out-of-ground effect case can be found in Ref. 9. CT is thrust coefficient. C1, C2 are instantaneous aerodynamic rolling and pitching moment coefficients expressed in the tip path plane. Obviously, they are time dependent for unsteady flight. The

subscript "aero" denotes that only the aerodynamic contribution is considered and the inertial part is not included. The "$\bullet$" denotes time derivative.

Due to the proximity of the rotor disk to the ship deck, the rotorcraft/ship interactions induce upwash at the rotor disk, thereby changing the total inflow and the inflow distribution over the rotor disk. Hence, the dynamic inflow model for the case of in-ground-effect model can be written as:

$$[M]_{ige} \{\dot{\lambda}\}_{ige} + [\hat{L}]_{ige}^{-1} \{\bar{\lambda}\}_{ige} = \{\{\bar{C}\}_{aero}\}_{ige} \quad (12)$$

where : $[M]_{ige}$, $[\hat{L}]_{ige}$ are the apparent mass and the inflow gain matrices for the case of in-ground-effect. Suppose

$$\left\{\bar{\lambda}\right\}_{ige} = \begin{bmatrix} g_1 & 0 & 0 \\ 0 & g_2 & 0 \\ 0 & 0 & g_3 \end{bmatrix} \left\{\bar{\lambda}\right\}_{oge} \quad (13)$$

and

$$\left\{\bar{C}\right\}_{ige} = \begin{bmatrix} h_1 & 0 & 0 \\ 0 & h_2 & 0 \\ 0 & 0 & h_3 \end{bmatrix} \left\{\bar{C}\right\}_{oge} \quad (14)$$

Thus, for trimmed flight with rotor treated as a disk, and noticing that the forcing functions (CT, C1, C2) are approximately the same for out-of-ground effect case and in-ground effect case. From Eqs. (12)-(14) with $h_i = 1$, $i = 1,2,3$ and $\dot{\bar{\lambda}} = 0$, we get

$$\left\{\hat{L}\right\}_{ige} = \begin{bmatrix} g_1 & 0 & 0 \\ 0 & g_2 & 0 \\ 0 & 0 & g_3 \end{bmatrix} \left\{\hat{L}\right\}_{oge} \quad (15)$$

Using results from CFD analysis for the ship ground effect cases of helicopter hovering over the ship deck at different positions and for different speeds, general expressions for g_i, $i = 1,2,3$ are obtained using curve fitting techniques. The resulting expression are obtained as

$$g_i = \frac{a_i(x,y) + \dfrac{b_i(x,y)}{h} + \dfrac{c_i(x,y)}{h^2} + \dfrac{d_i(x,y)}{h^3}}{k_{0_i} + k_{1_i}\mu + k_{2_i}\mu^2}, \quad i = 1,2,3 \quad (16)$$

where a_i, b_i, c_i, d_i are all cubic spline fitted functions of x and y. Thus, from equation (16), the correction factors g_1, g_2, g_3 that account for ground effect, are all functions of rotor position (x,y,z) with respect to ship deck and advance ratio. For comparison, the widely used Cheesemann & Bennett model [10] is of the form

$$g_i = 1. - \frac{1}{16h^2}\left(\frac{1}{1 + (\dfrac{\mu}{\lambda_{oge}})^2}\right), \quad i = 1,2,3 \quad (17)$$

Also, for comparison purpose, the variation of g_i (for the uniform component) is shown in Fig. 13 as computed using the Cheesemann & Bennett model and the new model, for cases of helicopter hovering at three different locations above the ship deck. From Fig. 13, it is clear that ship ground effect is different for different positions around the ship deck as predicted by the new model.
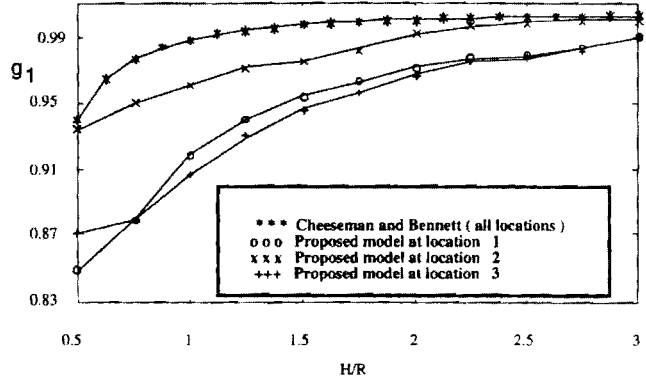
Figure 13. Comparison of Different Models

6. Conclusions

A ground effect model for rotorcraft/ship dynamic interface that is suitable for real time simulation purposes is developed in this paper. The gain matrix in the dynamic inflow model is identified as a function of the location of the rotor with respect to the ship deck, the height of the rotor above the deck and advance ratio. Also, the new model takes into account partial ground effect. However, the ship ground effect model developed in this study is only applicable for trimmed flight above the deck. Further work is needed to capture the unsteady effects due to heaving, rolling and/or pitching of the ship deck. Also, validation of the model using experimental data is needed.

6

References

1. Healey, J. Val., "Prospects for Simulating the Helicopter/Ship Interface," Naval Engineers Journal, Vol. 99, No. 2, March 1987, pp. 45-63.

2. Mello, O.A.F., Prasad, J.V.R., Sankar, L.N., and Tseng, W., "Analysis of Helicopter/Ship Aerodynamic Interactions," AHS Aeromechanics Specialists Conference, San Francisco, California, Jan. 1994.

3. Ferrir, B., and Semenza, J., "NATC Manned Flight Simulator VTOL Ship Motion Simulation and Application" 46th Annual Forum of AHS, Washington DC, 1990

4. Zhang H., Mello, O.A.F., Prasad, J.V.R., Sankar, L. N., and Funk, J. D. , "A Simulation Model of Ship Ground Effect For Rotorcraft/Ship Interaction Study," AHS 51st Annual Forum, Fort Worth, TX May 9-11,1995

5. Prasad, J.V.R., Manoj M., Mavris, D. and Zhang, H. , "Ship Airwake Simulation Models for Rotorcraft/Ship Interactions Study," AIAA 95-3406

6. Hess, J. L., and Smith, A. M O., " Calculation of Potential Flow About Arbitrary Bodies," Progress in Aeronautical Sciences, Vol. 8 Edited by D. Küchemann, Pergmon Press, Oxford, England, 1967

7. U.S. Department of Army-AFDD, " Second Generation Comprehensive Helicopter Analysis Systems, Version 2.1 " Vol. II, chapter 5, Moffett Field, CA July 1992

8. Kaplita,T.T., " UH-60A Black Hawk Engineering Simulation Method Validation and Proposed Modifications" Technical Report SER-70982, United Technologies Sikorsky Aircraft, June 1984.

9. Peters, D.A., and HaQuang, N., "Dynamic Inflow for Practical Applications" J. of AHS, Oct. 1988

10. Cheesemann, I.C. and Bennett, W.E., "The Effect of the Ground on a Helicopter Rotor in Forward Flight", ARC R&M No. 3021, Sept. 1955.

APPENDIX 4

1. INTRODUCTION

This report describes the modifications made in the helicopter simulation code GENHEL, in order to investigate helicopter/ship interactions. The theoretical formulation for the GENHEL code is given in Refs. 1 and 2 and will not be discussed here.

The effect of the ship proximity to the helicopter is modeled by using a standard panel method, based on the classical solution by Hess and Smith[7]. The ship is modeled by source panels which allow a good geometric representation. The effect of the ship on the rotor is given by the induced velocities on the rotor disk due to the ship panels. For the computation of the strengths of the sources, it is necessary to take into account both the ship velocity and the velocity field on the ship due to the rotor wake. This velocity field is computed using a rigid helical wake model. The strength of the rotor wake vortices depends on the circulation around the rotor blade, which, in turn, depends on the ship effects. Therefore, an iterative process would be needed. However, for the simulation problem, it may be assumed that changes in circulation around the blade and the flow about the ship are not too rapid and consequently the iterative process may be intrinsically performed during the simulation process.

For the computation of wake vorticity, two approaches have been employed: The first approach was to assume a prescribed vorticity distribution along the rotor disk. This allows all vorticity strengths on the disk and in the wake to be related to the thrust coefficient. Details on this approach were given in Ref. 4. The second approach was to compute the local vorticity at the rotor disk from the section lift. This approach requires numerical differentiation of the resulting vorticity distribution in order to obtain the wake vorticity strengths. Details on this latter approach are given in the Appendix.

In order to model the ground effect due to the sea surface, the method of images is used. An image rotor wake and an image ship panel system are placed below the sea surface and the influence of these images are taken into account in the computation of the downwash induced by the rotor and in the computation of the coefficient matrix for the ship panel method.

1

The remaining of this report is organized as follows: First, brief instructions on compiling and running GENHEL are given; Next the modifications and additions to GENHEL are described, including the first-order dynamic inflow model and the helicopter/ship interaction code using both the prescribed wake vorticity and computed wake vorticity models. Finally, an attempt to extend the rotor wake code to a free wake model is described.

2. COMPILING AND RUNNING GENHEL

The source code for the original version of GENHEL is divided into five FORTRAN files: bhawk.f, bhawka.f, bhawkb.f, bhawkc.f and bhawkd.f. The subroutine ROTOR is included in the file bhawkd.f and contains the blade-element model. In addition, several *.DAT files and a "Makefile" file are needed. The compilation is achieved by issuing the command Makefile twice to compile and link. This results in an executable file called bhawk. The execution is then performed by simply running bhawk. All the input files have their names pre-defined. The main input file is BHAWK.DAT. The input parameters in BHAWK.DAT are described in Ref. 1. Ref. 2 contains test cases that may be useful for validation of changes made to the original code.

3. FIRST-ORDER DYNAMIC INFLOW

The first order dynamic inflow model from Ref. 3 was implemented in GENHEL, as described in Ref. 4. These modifications were made mainly in the subroutines ROTOR and RADIAL, and a new subroutine called DYNINF was added. These changes were made in bhawkd.f, resulting in a new file called bhawkd2.f. Minor changes were made to the file bhawkc.f, for output of variables of interest, but this file was not renamed. A new Makefile2 file was used to compile and link this dynamic inflow version. Note that these files also include the turbulence modifications made by Riaz (Refs. 5,6).

4. HELICOPTER/SHIP INTERACTION: PRESCRIBED VORTICITY VERSION

The first version of the helicopter/ship interaction model was developed using a rigid helical wake model with prescribed vorticity distribution in the wake, as described in Ref. 4. The ship model was the panel method of Ref. 7. The rotor wake and ship models were included in the file bhawke.f. Changes were made in the file bhawkd2.f, resulting in a new file bhawkd3.f. Minor changes were also made in bhawk.f and bhawkb.f, resulting in bhawk2.f and bhawkb2.f, respectively. This version should be compiled and linked by issuing the command Makefile3 twice, which generates the executable file bhawk2. The changes are significantly commented (one can search for them by searching for the string MELLO).

4.1. Subroutines

The subroutines and function subprograms included in bhawke.f are as follows:

RSHIP   Main module for computation of the interaction between the rotor and the ship; calls other needed routines.

GETSHC   Reads ship coordinates and computes unit vectors.

EUL3   Constructs a matrix of coordinate transformations after 3 Euler rotations α about y, β about z' and γ about x".

MATMUL,   Subroutines for matrix multiplication.
MTMUL,
MTMUL2

CONV   Contains the convergence procedure for the integration which gives the velocity induced by the rotor wake at a given point.

AINTT   Function to be integrated along the wake coordinate to give total induced velocity due to wake tip vortex filaments.

5

GAMATV   Functional variation of trailing vorticity as a function of the sine and cosine of blade azimuth when the filament left the blade.

AINTB   Function to be integrated along the radius to give total induced velocity due to blade bound vortices on a given point.

GAMABV   Functional variation of bound vorticity as a function of the radius and sine and cosine of blade azimuth.

AINTNW   Function to be integrated along the near wake to give total induced velocity due to blade shed and trailing vortices on a given point; for a given wake age, it uses a radial integration of AINWR.

AINWR   Function to be integrated along the radius to give total induced velocity due to a blade shed vortex filament and due to the sum of trailing vortex elements at that near wake location on a given point.

GSHEDV   Functional variation of shed vorticity as a function of the radius and sine and cosine of blade azimuth.

GTRAV   Functional variation of trailing vorticity as a function of the radius and sine and cosine of blade azimuth.

GAULEG   Computes abscissas and weights for Gauss-Legendre quadrature (from Ref. 8).

QGAUS,   Integrate a function using Gauss-Legendre quadrature (from Ref. 8).
QGAUSR

PANEL   Contains the panel method procedure; calls subroutines for the several coordinate transformations and induced velocity computations. It computes the influence coefficients for induced velocities due to a ship panel on other ship panels and due to a ship panel on the rotor blade elements.

6

PANVEL   Computes the velocities induced by a ship panel, in the panel axes, on a point given in the same panel axes.

TRAFP   Performs coordinate transformations from ship axes to panel axes.

TRAPF   Performs coordinate transformations from panel axes to ship axes.

TRAFPM   Performs coordinate transformations from ship axes to mirror panel axes.

TRAPFM   Performs coordinate transformations from mirror panel axes to ship axes.

LUDCMP   Performs an LU decomposition of the ship influence coefficient matrix (from Ref. 8).

LUBKSB   Performs a back-substitution for solution of the system of equations, given the LU decomposition of the matrix of coefficients.

4.2. Input Parameters

The input parameters for the rotor/ship interaction computation are included in the file BHAWK.DAT and in a new file called rship.dat. The format of this latter file is as follows:

```
0.95  0.5   0.0   1.0   1.0   0.02  36  10  3     10
Rtv   Fnw   XnOfr Fnctr Kt    Eps   Nqn Nqr Nmin Nmax
```

The above parameters have the following meaning:

Rtv   Radial location of the tip vortex
Fnw   Length of near wake, in number of revolutions
XnOfr   Wake age for starting of integration
Fnctr   Wake age for wake contraction, in number of revolutions
Kt   Factor used in vorticity distribution (see Ref. 4)
Eps   Tolerance for convergence in wake integration
Nqn   Number of points along the wake for Gauss quadrature

7

Nqr   Number of points along the radius for Gauss quadrature

Nmin   Minimum number of revolutions for wake integration

Nmax   Maximum number of revolutions for wake integration

The additions to BHAWK.DAT are as follows: The following flags are added to $RUNFLAG:

IGNDEF Ground effect flag (0 for no ground effect)

ISHIP   Ship flag (0 for no ship)

IRRW   Rotor induced velocity flag: If set to 1, rotor wake is used to compute inflow on rotor disk; if set to 0, dynamic inflow is used. Recommended setting is 0.

ISHMV   Ship mean velocities flag: If set to 1, the ship airwake mean velocities are obtained from polynomial fitting of test data; if set to 0, the panel method is used. Recommended setting is 1.

and the following inputs are included in $RUNIC:

ALSHIP   Ship attitude (deg)

PHSHIP   Ship bank angle (deg)

VSHKT   Ship velocity (knots)

XSHIP0, Initial ship location in inertial reference frame.
YSHIP0,
ZSHIP0

VWIND   Wind velocity (knots)

PSIWND   Wind direction (deg)

NSS   Number of blade elements (was fixed in the code in the original version).

8

5. HELICOPTER/SHIP INTERACTION: COMPUTED VORTICITY VERSION

Another version of the helicopter/ship interaction model was developed using the same rigid helical wake model as above, but with the vorticity distribution in the wake computed from the section lift coefficients. Details on this model are given in the Appendix.

The changes in the rotor wake model resulted in a new file bhawke2.f, which replaced bhawke.f. Changes were also made in bhawkd3.f, resulting in a new file bhawkd4.f, primarily to compute the section lift and pass it to the rotor wake code. This version should be compiled and linked by issuing the command Makefile4 twice, which generates the executable file bhawk3.

For all versions of the helicopter/ship interaction code discussed so far, the rotor wake was simply truncated at a small height above the ship deck. It was observed that this procedure resulted in unrealistic ground effect modeling at very low heights. Consequently, a new version was developed in which the wake was not truncated, but assumed to be "flat", i.e., in a plane parallel to the ground, just above it, for wake ages above the wake age for which the vortex wake filaments were at a specified minimum distance from the deck (see Fig. 1). These changes were implemented in a new file bhawke3.f, which replaced bhawke2.f. This version should be compiled and linked by issuing the command Makefile6 twice, which generates the executable file bhawk6. This is to be considered the current production version.

Clearance

Flat wake near ground
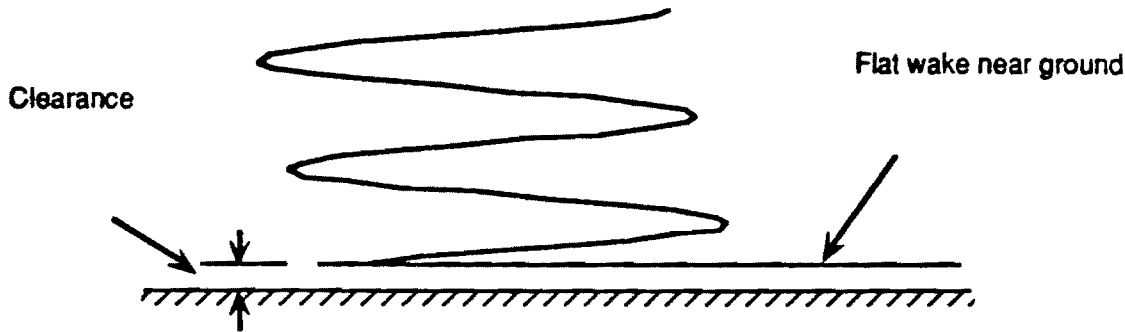
Fig. 1: Modified Wake Geometry

5.1. Subroutines

The subroutines and function subprograms in bhawke2.f and bhawke3.f are essentially the same as in bhawke.f and are listed below:

RSHIP   Main module for computation of the interaction between the rotor and the ship; calls other needed routines.

GETSHC   Reads ship coordinates and computes unit vectors.

EUL3   Constructs a matrix of coordinate transformations after 3 Euler rotations α about y, β about z' and γ about x".

MATMUL,   Subroutines for matrix multiplication.
MTMUL,
MTMUL2

GAMABV   Functional variation of bound vorticity as a function of the radius and sine and cosine of blade azimuth.

GSHEDV   Functional variation of shed vorticity as a function of the radius and sine and cosine of blade azimuth.

GTRAV   Functional variation of trailing vorticity as a function of the radius and sine and cosine of blade azimuth.

10

GAMATV   Functional variation of trailing vorticity as a function of the sine and cosine of blade azimuth when the filament left the blade.

BVINT   Subroutine for integration of bound vortices' contribution using trapezoidal rule.

AINTB   Function to be integrated along the radius to give total induced velocity due to blade bound vortices on a given point.

NWINT   Subroutine for integration along near wake.

AINTNW   Function to be integrated along the near wake to give total induced velocity due to blade shed and trailing vortices on a given point; for a given wake age, it uses a radial integration of AINWR.

AINWR   Function to be integrated along the radius to give total induced velocity due to a blade shed vortex filament and due to the sum of trailing vortex elements at that near wake location on a given point.

FWINT   Subroutine for integration along far wake.

AINTT   Function to be integrated along the wake coordinate to give total induced velocity due to wake tip vortex filaments.

CONV   Integration routines not used in these versions
GAULEG,
QGAUS,
QGAUSR

PANEL   Contains the panel method procedure; calls subroutines for the several coordinate transformations and induced velocity computations. It computes the influence coefficients for induced velocities due to a ship panel on other ship panels and due to a ship panel on the rotor blade elements.

PANVEL   Computes the velocities induced by a ship panel, in the panel axes, on a point given in the same panel axes.

11

TRAFP   Performs coordinate transformations from ship axes to panel axes.

TRAPF   Performs coordinate transformations from panel axes to ship axes.

TRAFPM   Performs coordinate transformations from ship axes to mirror panel axes.

TRAPFM   Performs coordinate transformations from mirror panel axes to ship axes.

LUDCMP   Performs an LU decomposition of the ship influence coefficient matrix (from Ref. 8).

LUBKSB   Performs a back-substitution for solution of the system of equations, given the LU decomposition of the matrix of coefficients.

5.2. Input Parameters

As in the prescribed vorticity version, the input parameters for the rotor/ship interaction computation are included in the file BHAWK.DAT and in a new file called rship.dat. The format of this latter file is as follows:

```
0.95  0.5   0.0   1.0   1.0   0.02  36  10  3    10   0.1
Rtv   Fnw   XnOfr Fnctr Kt    Eps   Nqn Nqr Nmin Nmax Gndclf
```

The above parameters have the following meaning:

Rtv   Radial location of the tip vortex

Fnw   Length of near wake, in number of revolutions

XnOfr   Wake age for starting of integration

Fnctr   Wake age for wake contraction, in number of revolutions

Kt   Factor used in vorticity distribution (not used in this version)

Eps   Tolerance for convergence in wake integration (not used in this version)

Nqn   Number of points along the wake for Gauss quadrature (not used in this version)

Nqr   Number of points along the radius for Gauss quadrature (not used in this version)

12

Nmin   Minimum number of revolutions for wake integration

Nmax   Maximum number of revolutions for wake integration

Gndclf Wake clearance above deck (minimum distance between wake filaments and deck), non-dimensionalized by the rotor radius.

Note that the format of the input file is the same as in the previous version, with the addition of Gndclf. The unused input parameters were maintained for compatibility with the previous version.

The additions to BHAWK.DAT are as in the previous version: The following flags are added to $RUNFLAG:

IGNDEF Ground effect flag (0 for no ground effect)

ISHIP   Ship flag (0 for no ship)

IRRW   Rotor induced velocity flag: If set to 1, rotor wake is used to compute inflow on rotor disk; if set to 0, dynamic inflow is used. Recommended setting is 0.

ISHMV   Ship mean velocities flag: If set to 1, the ship airwake mean velocities are obtained from polynomial fitting of test data; if set to 0, the panel method is used. Recommended setting is 1.

and the following inputs are included in $RUNIC:

ALSHIP Ship attitude (deg)

PHSHIP Ship bank angle (deg)

VSHKT   Ship velocity (knots)

XSHIP0, Initial ship location in inertial reference frame.
YSHIP0,
ZSHIP0

VWIND   Wind velocity (knots)

PSIWND Wind direction (deg)

NSS   Number of blade elements (was fixed in the code in the original version).

5.3. Parametric Investigation

A limited parametric investigation was performed to determine the effect of number of revolutions and wake clearance above the ground on the ground effect modeling. Representative results are shown in Figs. 2 and 3. In these figures the power required is non-dimensionalized by the hover out-of-ground effect (OGE) power required and plotted as a function of the reduced advance ratio, $\mu/(C_T/2)^{1/2}$. These non-dimensionalizations allow a more meaningful comparison with the experimental data in Ref. 10, which were obtained for the Boeing-Vertol YUH-61, a helicopter of the same class as the UH-60.

From the parametric investigation, it may be concluded that the clearance above the ground is a minor factor, at least in the range investigated. The number of revolutions is a major factor at low speeds, and a minor factor at high speeds, because as the speed is increased, the wake is washed away from the deck.
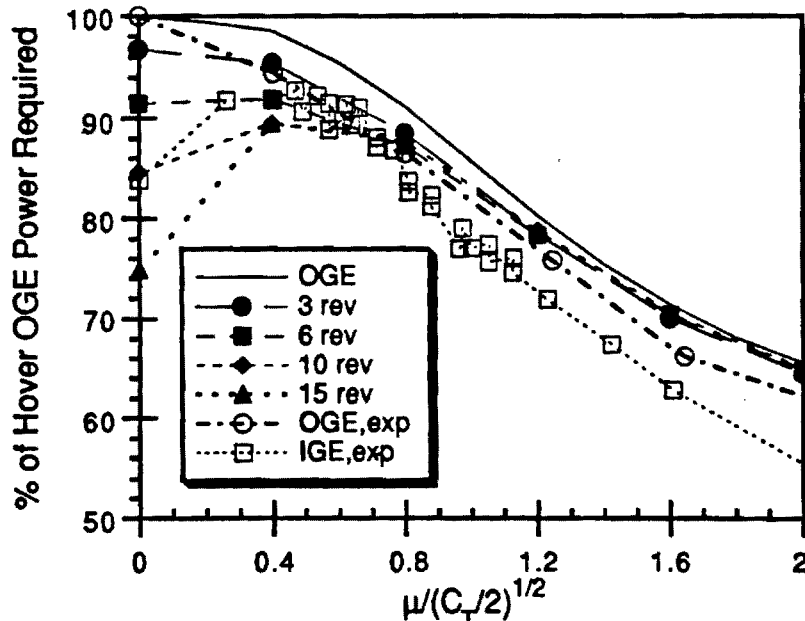

Fig. 2: Parametric Investigation: Effect of Number of Wake Revolutions.
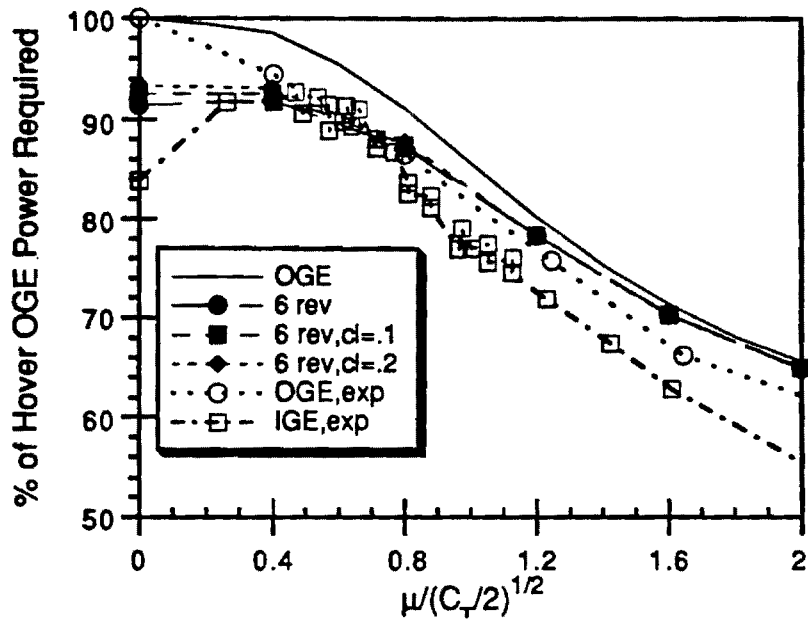
Fig. 3: Parametric Investigation: Effect of Clearance above Ground.

6. HELICOPTER/SHIP INTERACTION: FREE WAKE MODEL

In order to increase the code fidelity at very low speeds, an extension of the current code to a free wake model has been attempted. The changes in the rotor wake model resulted in a new file bhawke4.f. Preliminary runs showed that the wake was unstable, even though relaxation techniques were used. This is illustrated in Fig. 4, where side views of a wake filament from one blade is shown at four iteration levels. This unstable behavior has been observed during the development of other free wake codes. From these preliminary computations, it became apparent that the further development of a free wake code would require a substantial effort by itself, in a deviation from the main objective at hand, which is the helicopter/ship interaction study. Therefore, it is recommended that the emphasis be shifted towards the adaptation of the existing free wake module in CAMRAD for application to the helicopter/ship interaction study.

Fig. 4: Free Wake Instability

16

APPENDIX

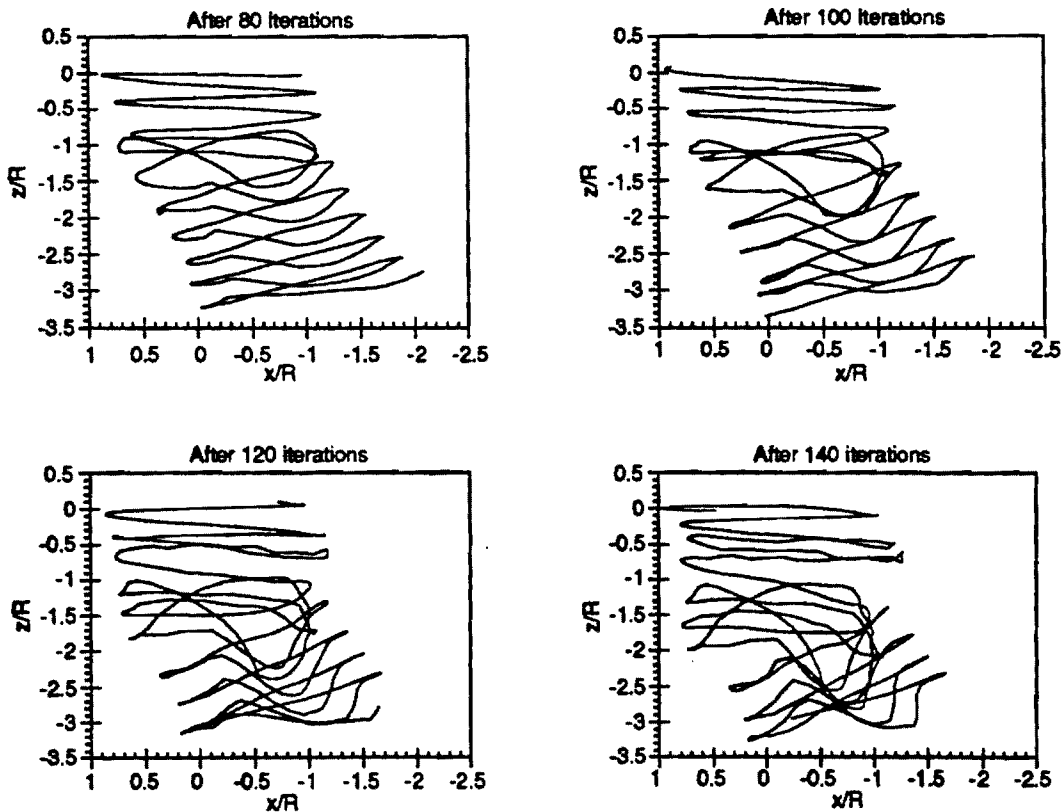# SHIP GROUND EFFECT MODELING USING PRESCRIBED WAKE GEOMETRY WITH COMPUTED WAKE VORTICITY DISTRIBUTION

The effect of the ship proximity to the helicopter is modeled by using a standard panel method, based on the classical solution by Hess and Smith[7]. The ship is modeled by source panels which allow a good geometric representation. The effect of the ship on the rotor is given by the induced velocities on the rotor disk due to the ship panels. For the computation of the strengths of the sources, it is necessary to take into account both the ship velocity and the velocity field on the ship due to the rotor wake. This velocity field is computed using a rigid helical wake model. The strength of the rotor wake vortices depends on the circulation around the rotor blade, which, in turn, depends on the ship effects. Therefore, an iterative process would be needed. However, for the simulation problem, it may be assumed that changes in circulation around the blade and the flow about the ship are not too rapid and consequently the iterative process may be intrinsically performed during the simulation process.

In order to model the ground effect due to the sea surface, the method of images is used. An image rotor wake and an image ship panel system are placed below the sea surface and the influence of these images are taken into account in the computation of the downwash induced by the rotor and in the computation of the coefficient matrix for the ship panel method.

A.1. Ship Formulation

The ship surface is approximately represented by plane source panels with constant distributed strength. The strengths of the sources are determined by enforcing the non-penetration condition at the centroid of each panel. In this implementation, both the normal component of the ship's motion and the normal component of the downwash induced by the rotor are taken into account. The details of the ship source panel method

17

are given in Ref. 7 and therefore will not be repeated here. This formulation results in a linear system of equations to be solved for the ship panel source strengths σ:

$$[A]\{\sigma\} = [B] \qquad (A.1)$$

where [A] is the matrix of influence coefficients, {σ} is the vector of unknown source strengths and [B] is the right-hand side which includes the normal component of the velocities on the ship surface due to the free-stream and due to the rotor and its wake. The system of equations (A.1) is solved by a standard linear equations solver. The resulting source panel strengths are then used to compute the velocities induced by the ship source panel system on the rotor disk.

A.2. Rotor Wake Formulation

In order to compute the induced velocity due to the rotor and its wake on the ship, as well the rotor disk inflow distribution in ground effect, a rigid wake model is used. This model is a modified version of the model described in Ref. 4 and allows the computation of the instantaneous induced velocities both on the rotor disk and on the ship surface. In Ref. 4 a prescribed vorticity distribution was assumed. In the current version, the vorticity distribution is computed from the blade section lift, as described in more detail in Section A.2.1. It should also be noted that in the present work the rotor wake model is used only for computation of the induced velocities on the ship surface. Numerical experimentation has shown that using the current model for computation of induced velocities on the rotor disk is computationally time-consuming while presenting no clear advantage over a dynamic inflow model.

The following assumptions are made:

1) Blade flapping angles are small and their higher harmonics are negligible;

2) The rotor blade is modeled by a lifting line of bound vorticity; this bound vorticity is related to the blade section lift by Kutta-Joukowski's theorem;

3) The wake has a prescribed geometry, which is basically a classical skewed helical wake, with a limited wake contraction model;

18

4) The wake is divided into a "near" wake, composed of trailing and shed vortices and a "far" wake composed of trailing tip vortices only. The strengths of the trailing and shed vortices are given by the radial and azimuth-wise variations of the bound vorticity, respectively, while the strength of the far wake tip vortex is assumed as equal to the maximum bound vorticity at the azimuth location where the vortex filament leaves the blade;

5) The rotor wake is convected downstream with a velocity which is equal to the vector sum of the free stream velocity and the averaged (momentum theory value) induced velocity over the disk.

A.2.1. Vorticity Distribution

The blade bound vorticity distribution is obtained through an iterative process from the blade section lift. Let the blade section bound vorticity be $\Gamma_{b_{ij}} = \Gamma_b(r_i, \psi_j)$. From Kutta-Joukowski theorem:

$$l_{ij} = \rho \, V_{ij} \, \Gamma_{ij} = \rho \, (\Omega R)(\bar{r}_i + \mu \sin \psi_j) \, \Gamma_{b_{ij}} \tag{A.2}$$

or:

$$\Gamma_{b_{ij}} = \frac{\ell_{ij}}{\rho(\Omega R)(\bar{r}_i + \mu \sin \psi_j)} \tag{A.3}$$

A.2.2. Velocity Induced by Blade Bound Vortices

From the computed bound vorticity distribution, the velocity induced by the blade bound vortices can be obtained by application of the Biot-Savart law:

$$v_b = \frac{1}{4\pi} \int_{\bar{r}=0}^{1} \Gamma_b \frac{\vec{ds_b} \times \Delta \vec{R}_{Pb}}{|\Delta \vec{R}_{Pb}|^3} \tag{A.4}$$

where $d\vec{s}_b$ is the elementary vector in the direction of the vortex filament and $\Delta\vec{R}_{Pb}$ is the position vector of the point in question with respect to the bound vortex element. Denoting by $\vec{R}_b$ the position vector of a blade bound vortex element as expressed in the tip-path-plane (TPP) reference frame:

$$\vec{R}_b = r \left\{ \left[-\cos\psi\, \hat{i}_T - \sin\psi\, \hat{j}_T \right] \cos\beta_0 + \sin\beta_0\, \hat{k}_T \right\} \tag{A.5}$$

Then the elementary vector $d\vec{s}_b$ can be obtained from:

$$d\vec{s}_b = \frac{\dfrac{\partial\vec{R}_b}{\partial r}}{\left| \dfrac{\partial\vec{R}_b}{\partial r} \right|} dr \tag{A.6}$$

with

$$\frac{\partial\vec{R}_b}{\partial r} = \left[-\cos\psi\, \hat{i}_T - \sin\psi\, \hat{j}_T \right] \cos\beta_0 + \sin\beta_0\, \hat{k}_T = \frac{\vec{R}_b}{r} \tag{A.7}$$

Given a point with coordinates (x_P, y_P, z_P) in the tip-path-plane reference frame, the vector $\Delta\vec{R}_{Pb}$ is then:

$$\Delta\vec{R}_{Pb} = \vec{R}_P - \vec{R}_b = \left(x_P\, \hat{i}_T + y_P\, \hat{j}_T + z_P\, \hat{k}_T \right) - \vec{R}_b \tag{A.8}$$

The discretization of Eqs (A.5–A.8) is straightforward. Eq. (A.4) then reduces to a summation over the blade:

$$v_b\!\left(\psi_j, \vec{R}_P\right) = v_{b_j} = \frac{1}{4\pi} \sum_{i=1}^{N_r} \Gamma_{b_{ij}} \frac{\Delta\vec{s}_{b_i} \times \Delta\vec{R}_{Pb_{ij}}}{\left|\Delta\vec{R}_{Pb_{ij}}\right|^3} \tag{A.9}$$

A.2.3. Near Wake

As mentioned above, the near wake is assumed to be composed of trailing and shed vortices, with strength given by the radial and azimuth-wise variations of the bound

vorticity, respectively, at the azimuth location where the vortex filament leaves the blade. Let us first consider an element of a trailing vortex filament of length $r_i \Delta v$, which left the blade at the radial location r_i, and is located at a wake age v_k. This element has left the blade when it was at an azimuth location $\psi_j - v_k$, ψ_j being the current azimuth location of the blade. Therefore, the vorticity of the element is given by $\Gamma_t (r_i, \psi_j - v_k) r_i \Delta v$, where $\Gamma_{t_{i,j,k}} = \Gamma_t (r_i, \psi_j - v_k)$ is the trailing vortex vorticity, equal to the radial variation of Γ_b:

$$\Gamma_{t_{i,k}} = \Gamma_t\left(\bar{r}_i, \psi_j - v_k\right) = \frac{\partial \Gamma_b}{\partial \bar{r}} \approx \frac{\Gamma_b\left(\bar{r}_i, \psi_j - v_k\right) - \Gamma_b\left(\bar{r}_{i-1}, \psi_j - v_k\right)}{\bar{r}_i - \bar{r}_{i-1}} \qquad (A.10)$$

The velocity induced by the entire filament at a point is given by integration of elementary induced velocities obtained from the Biot-Savart law:

$$dv_t = \frac{1}{4\pi} \int_{v=0}^{v_m} \Gamma_t \frac{d\vec{s}_t \times \Delta \vec{R}_{Pt}}{\left|\Delta \vec{R}_{Pt}\right|^\beta} \qquad (A.11)$$

where $d\vec{s}_t$ is the elementary vector in the direction of the vortex filament and $\Delta \vec{R}_{Pt}$ is the position vector of the point in question with respect to the vortex element. Note that the integration is performed only along the "near" wake. Note also that Eq.(A.11) gives only the velocity induced by a single trailing vortex filament. To obtain the total induced velocity due to all trailing vortex filaments, one has to integrate Eq.(A.11) along the blade, i.e.:

$$v_t = \frac{1}{4\pi} \int_{\bar{r}=0}^{1} \int_{v=0}^{v_m} \Gamma_t \frac{d\vec{s}_t \times \Delta \vec{R}_{Pt}}{\left|\Delta \vec{R}_{Pt}\right|^\beta} \qquad (A.12)$$

Denoting by $\vec{R}_s$ the position vector of the trailing vortex element as expressed in the tip-path-plane (TPP) reference frame and using the assumption that the wake is convected downstream with a velocity which is equal to the vector sum of the free stream velocity and the averaged induced velocity over the disk, we have:

$$\vec{R}_s = r \left\{\left[- \cos (\psi\text{-}v)\,\hat{i}_T - \sin (\psi\text{-}v)\,\hat{j}_T\right] \cos \beta_0 + \sin \beta_0 \; \hat{k}_T\right\} + \frac{\vec{V}_\infty - \vec{V}_{Ht}}{\Omega} v \qquad (A.13)$$

21

where β_0 is the coning angle, Ω is the rotor rotational speed, $\vec{V}_{H_T}$ is the helicopter velocity vector in the TPP reference frame, $\hat{i}_T$, $\hat{j}_T$ and $\hat{k}_T$ are the unit vectors corresponding to the TPP axes, and $\vec{v}_{i_0}$ is the averaged induced inflow vector, given by:

$$\vec{v}_{i_0} = - (\Omega R) \lambda_{i_0} \hat{k}_T \tag{A.14}$$

where λ_{i_0} is the induced inflow ratio. The elementary vector in the direction of the filament, $\vec{ds}_l$, can be obtained as:

$$\vec{ds}_l = \frac{\dfrac{\partial \vec{R}_s}{\partial v}}{\left| \dfrac{\partial \vec{R}_s}{\partial v} \right|} r \, dv \tag{A.15}$$

with

$$\frac{\partial \vec{R}_s}{\partial v} = r \left[- \sin(\psi - v) \hat{i}_T + \cos(\psi - v) \hat{j}_T \right] \cos \beta_0 + \frac{\vec{v}_{i_0} - \vec{V}_{H_T}}{\Omega} \tag{A.16}$$

Given a point with coordinates (x_P, y_P, z_P) in the tip-path-plane reference frame, the vector $\Delta \vec{R}_{P_l}$ is then:

$$\Delta \vec{R}_{P_l} = \vec{R}_P - \vec{R}_s = \left(x_P \hat{i}_T + y_P \hat{j}_T + z_P \hat{k}_T \right) - \vec{R}_s \tag{A.17}$$

The discretization of Eqs (A.13–A.17) is straightforward. Eq. (A.12) then reduces to a double summation over the radial and wake coordinates along the near wake:

$$v_l(\psi_j, \vec{R}_P) = v_{l_j} = \frac{1}{4\pi} \sum_{k=1}^{N_{nw}} \sum_{i=1}^{N_r} \Gamma_{l_{ijk}} \frac{\Delta \vec{s}_{l_{ijk}} \times \Delta \vec{R}_{P_{l_{ijk}}}}{\left| \Delta \vec{R}_{P_{l_{ijk}}} \right|^3} \tag{A.18}$$

Now, let us consider an element of a shed vortex filament of length Δr_i, which left the blade at the radial location r_i, and is located at a wake age v_k. This element has left the blade when it was at an azimuth location $\psi_j - v_k$, ψ_j being the current azimuth location

22

of the blade. Therefore, the vorticity of the element is given by $\Gamma_s \, (\bar{r}_i, \psi_j - v_k) \, \Delta r_i$, where Γ_s $(\bar{r}_i, \psi_j - v_k)$ is the shed vortex vorticity, equal to the azimuthal variation of Γ_b:

$$\Gamma_{s_\phi} = \Gamma_s \left(\bar{r}_i, \psi_j - v_k \right) = \frac{\partial \Gamma_b}{\partial \psi} \approx \frac{\Gamma_b \left(\bar{r}_i, \psi_j - v_k \right) - \Gamma_b \left(\bar{r}_i, \psi_{j-1} - v_k \right)}{\Delta \psi} \qquad (A.19)$$

The velocity induced by the entire shed vortex system at a point is given by radial integration of elementary induced velocities obtained from the Biot-Savart law, and subsequent integration along the wake to account for all the shed vortices:

$$v_s = \frac{1}{4\pi} \int_{v=0}^{v_m} \int_{\bar{r}=0}^{1} \Gamma_s \frac{\vec{ds}_s \times \Delta \vec{R}_{Ps}}{\left| \Delta \vec{R}_{Ps} \right|^\beta} \qquad (A.20)$$

Note that the integration is performed only along the "near" wake. The position vector of the shed vortex element, $\vec{R}_s$, is given again by Eq. (A.13), therefore the vector $\Delta \vec{R}_{Ps}$ is equal to $\Delta \vec{R}_{Pt}$ and is accordingly given by Eq. (A.17). The elementary vector in the direction of the shed vortex filament, $\vec{ds}_s$, can be obtained as:

$$\vec{ds}_s = \frac{\dfrac{\partial \vec{R}_s}{\partial r}}{\left| \dfrac{\partial \vec{R}_s}{\partial r} \right|} dr \qquad (A.21)$$

with

$$\frac{\partial \vec{R}_s}{\partial r} = \left[- \cos{(\psi \text{-} v)} \, \hat{i}_T - \sin{(\psi \text{-} v)} \, \hat{j}_T \right] \cos{\beta_0} + \sin{\beta_0} \; \hat{k}_T \qquad (A.22)$$

The discretization of Eq (A.22) is straightforward. Eq. (A.20) then reduces to a double summation over the radial and wake coordinates along the near wake:

$$v_s \left(\psi_j, \vec{R}_P \right) = v_{s_j} = \frac{1}{4\pi} \sum_{k=1}^{N_{sw}} \sum_{i=1}^{N_s} \Gamma_{s_{ijk}} \frac{\Delta \vec{s}_{s_{ijk}} \times \Delta \vec{R}_{Ps_{ijk}}}{\left| \Delta \vec{R}_{Ps_{ijk}} \right|^\beta} \qquad (A.23)$$

23

A.2.4. Far Wake

As mentioned above, the far wake is assumed to be composed of trailing tip vortices only, with strength assumed as equal to the maximum bound vorticity at the azimuth location where the vortex filament leaves the blade. Considering an element of wake filament of length $r_{tv} \Delta v$ (where r_{tv} corresponds to the radial location where the tip vortex has rolled up) and at a wake age v_k, this element has left the blade when it was at an azimuth location $\psi_j - v_k$, ψ_j being the current azimuth location of the blade. Therefore, the vorticity of the element is given by $\Gamma_{T_{jk}} r_{tv} \Delta v = \Gamma_T (\psi_j - v_k) r_{tv} \Delta v$, where $\Gamma_T (\psi_j - v_k)$ is the trailing tip vortex vorticity, equal to the radial maximum of Γ_b:

$$\Gamma_{T_{jk}} = \Gamma_T(\psi_j - v_k) = \max_i \Gamma_b(\bar{r}_i, \psi_j - v_k) \tag{A.24}$$

The velocity induced by the wake at a point is given by integration of elementary induced velocities obtained from the Biot-Savart law:

$$v_T = \frac{1}{4\pi} \int_{-\infty}^{\infty} \Gamma_T \frac{\vec{ds}_T \times \Delta \vec{R}_{PT}}{|\Delta \vec{R}_{PT}|^3} \tag{A.25}$$

where $\vec{ds}_T$ is the elementary vector in the direction of the vortex filament and $\Delta \vec{R}_{PT}$ is the position vector of the point in question with respect to the vortex element. Denoting by $\vec{R}_T$ the position vector of the tip vortex element as expressed in the tip-path-plane (TPP) reference frame and using the assumption that the wake is convected downstream with a velocity which is equal to the vector sum of the free stream velocity and the averaged induced velocity over the disk, we have:

$$\vec{R}_T = r_{tv} \left\{ \left[-\cos(\psi - v)\,\hat{i}_T - \sin(\psi - v)\,\hat{j}_T \right] \cos \beta_0 + \sin \beta_0 \, \hat{k}_T \right\} + \frac{\vec{V}_{i_0} - \vec{V}_{H_T}}{\Omega} v \tag{A.26}$$

The elementary vector in the direction of the tip vortex filament, $\vec{ds}_T$, can be obtained as:

24

$$d\vec{s}_T = \frac{\dfrac{\partial \vec{R}_T}{\partial v}}{\left|\dfrac{\partial \vec{R}_T}{\partial v}\right|} r_{tv}\, dv \qquad (A.27)$$

with

$$\frac{\partial \vec{R}_T}{\partial v} = r_{tv}\left[-\sin(\psi\text{-}v)\,\hat{i}_T + \cos(\psi\text{-}v)\,\hat{j}_T\right]\cos\beta_0 + \frac{\vec{V}_{i_0} - \vec{V}_{H_T}}{\Omega} \qquad (A.28)$$

Given a point with coordinates (x_P, y_P, z_P) in the tip-path-plane reference frame, the vector $\Delta\vec{R}_{PT}$ is then:

$$\Delta\vec{R}_{PT} = \vec{R}_P - \vec{R}_T = \left(x_P\,\hat{i}_T + y_P\,\hat{j}_T + z_P\,\hat{k}_T\right) - \vec{R}_T \qquad (A.29)$$

The discretization of Eqs (A.26–A.29) is straightforward. Eq. (A.25) then reduces to a summation over the wake coordinate along the far wake:

$$v_T\!\left(\psi_j, \vec{R}_P\right) = v_{T_j} = \frac{1}{4\pi}\sum_{k=N_{nw}+1}^{N_w} \Gamma_{T_k}\frac{\Delta\vec{s}_{T_k} \times \Delta\vec{R}_{PT_k}}{\left|\Delta\vec{R}_{PT_k}\right|^\beta} \qquad (A.30)$$

A.2.5. Vortex Core Model

A Rankine vortex core model[9] with radius of one tenth of the blade chord is used. This model is illustrated in Fig. A.1, and is applied by scaling the induced velocity due to the elementary vortex filament by the square of the ratio between the distance to the filament and the core radius, whenever the point where the induced velocity is being calculated lies within the vortex core.
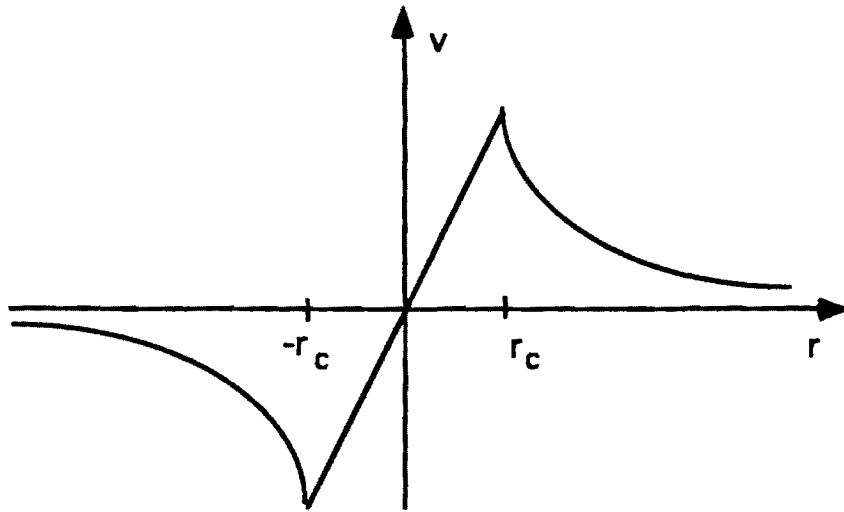
25

Fig. A.1: Rankine Vortex Core Model

REFERENCES

1. Howlett, J. J., "UH-60A Black Hawk Engineering Simulation Program: Volume I — Mathematical Model," NASA CR-166309, 1981.

2. Ballin, M. G., "Validation of Real-Time Engineering Simulation of the UH-60A Helicopter," NASA TM-88360, February 1987.

3. Peters, D. A., and HaQuang, N., "Dynamic Inflow for Practical Applications," *Journal of the American Helicopter Society*, October 1988, pp. 64–68.

4. Mello, O. A. F., "Numerical Simulation of Helicopter / Ship Airwake Interactions," Research Report submitted to Naval Air Warfare Center, School of Aerospace Engineering, Georgia Institute of Technology, Atlanta, July 1993.

5. Riaz, J., Prasad, J. V. R., Schrage, D. P., and Gaonkar, G. H., "New Method for Simulating Atmospheric Turbulence for Rotorcraft Applications," 47th Annual Forum of the American Helicopter Society, Phoenix, Arizona, 1991.

6. Riaz, Jamshed, "A Simulation Model of Atmospheric Turbulence for Rotorcraft Applications," Ph.D. Thesis, Georgia Institute of Technology, Atlanta, 1992.

7. Hess, J. L., and Smith, A. M. O., "Calculation of Potential Flow about Arbitrary Bodies," *Progress in Aeronautical Sciences*, Vol. 8. Edited by D. Küchemann. Pergamon Press, Oxford, England, 1967.

8. Press, W. H., Flannery, B. P., Teukolsky, S. A. and Vetterling, W. T., *Numerical Recipes — The Art of Scientific Computing (FORTRAN Version)*, Cambridge University Press, 1989.

9. U.S. Department of the Army — Aeroflightdynamics Directorate, "2GCHAS Theory Manual," (Second Generation Comprehensive Helicopter Analysis System, Version 2.1), Vol. II, Chapter 5 – Airloads and Induced Velocity, Ames Research Center, Moffett Field, CA, July 1992.

10. Sheridan, P. F., and Wiesner, W., "Aerodynamics of Helicopter Flight Near the Ground," 33rd Annual Forum of the American Helicopter Society, 1977.

11. Johnson, W., "A Comprehensive Analytical Model of Rotorcraft Aerodynamics and Dynamics, Part I: Analysis Development," NASA TM-81182, Part 1, June 1980.